UNIVERSITY **POLITEHNICA** of BUCHAREST

Faculty of Chemical Engineering and Biotechnologies

Department of Analytical Chemistry and Environmental Engineering

Doctoral School of Chemical Engineering and Biotechnologies

# PhD THESIS SUMMARY

## CHEMICALLY MODIFIED ELECTRODES WITH APPLICATIONS IN THE CONTROL OF SOIL AND PLANT POLLUTION WITH INORGANIC POLLUTANTS IN THE SLATINA INDUSTRIAL AREA

**PhD Supervisor:**
Professor Emeritus Elena DIACU, PhD Chem

**Doctoral Candidate:**
Chem. Adina-Maria SPIRIDON (PĂUN)

### PhD ASSESSMENT COMMITTEE

| | | | |
|---|---|---|---|
| **Chairwoman** | **Professor Alina Catrinel ION, PhD Eng** | **from** | **University POLITEHNICA of Bucharest** |
| **PhD Supervisor** | **Professor Emeritus Elena DIACU, PhD Chem** | **from** | **University POLITEHNICA of Bucharest** |
| **Referent** | **Professor Lucia MUTIHAC, PhD** | **from** | **University of Bucharest** |
| **Referent** | **Professor Emeritus Eleonora-Mihaela UNGUREANU, PhD Eng** | **from** | **University POLITEHNICA of Bucharest** |
| **Referent** | **Professor Gabriela STANCIU, PhD Eng** | **from** | **University "Ovidius" of Constanța** |

**Bucharest 2023**

# CONTENTS*

*The table of contents respects the pagination in the PhD thesis. Also, the numbers of the figures, tables, equations and bibliography sources in this summary correspond to those in the PhD thesis.

**Keywords**: chemically modified electrodes, E-5-((5-isopropyl-3,8-dimethylazulen-1-yl)diazenyl)-1H-tetrazole, 4-(azulen-1-yl)-2,6-bis((E)-2-(thiophen-2-yl)vinyl)pyridine, cyclic voltammetry, differential pulse voltammetry, anodic stripping voltammetry, scanning electron microscopy, atomic force microscopy.

# ACKNOWLEDGEMENTS

At the end of the doctoral internship, I would like to address a few words to express my gratitude to those who have supported and encouraged me in my scientific endeavor.

I sincerely and gratefully wish to thank my scientific tutor, Professor Emeritus Elena DIACU, PhD, from the Department of Analytical Chemistry and Environmental Engineering, Faculty of Chemical Engineering and Biotechnologies, University POLITEHNICA of Bucharest, for the trust I enjoyed as a PhD student, the patience, encouragement and professional competence she guided me with throughout this period.

Equally, I express my gratitude and thank Professor Emeritus Eleonora-Mihaela UNGUREANU, PhD Eng, from the Department of Inorganic Chemistry, Physical Chemistry and Electrochemistry, Faculty of Chemical Engineering and Biotechnologies, University POLITEHNICA of Bucharest, for the professionalism shown and the moral and professional support she has given me as a member of my guidance committee.

I would also like to thank the members of the PhD assessment committee: Professor Alina Catrinel ION, PhD Eng, Professor Lucia MUTIHAC, PhD, Professor Emeritus Eleonora-Mihaela UNGUREANU, PhD Eng, and Professor Gabriela STANCIU, PhD Eng, for their kindness to accept the task of evaluating my PhD thesis and to the members of my guidance committee consisting of Professor Emeritus Eleonora-Mihaela UNGUREANU, PhD Eng, Professor Lucia MUTIHAC, PhD, and Professor Daniela Simina ȘTEFAN, PhD Eng, for the advice and encouragement they gave me throughout the doctoral internship.

I am grateful and I thank all my fellow PhD students at the laboratory of *Electrochemical Processes in Organic Solvents (EPOS)* - Department of Inorganic Chemistry, Physical Chemistry and Electrochemistry of the Faculty of Chemical Engineering and Biotechnologies, for the support provided in carrying out laboratory experiments and for the scientific collaboration in writing the published articles. I would like to warmly thank Mrs Magdalena-Rodica BUJDUVEANU, PhD Eng, for the professional collaboration and good communication we enjoyed together.

Moreover, I would like to thank the specialists of the *C. D. Nenitescu* Center for Organic Chemistry - Romanian Academy for the professional competence proven in the synthesis of the azulenic derivatives studied in this thesis and in the published scientific articles.

My good thoughts and words of thanks go to my family and collaborators at the high school where I work as a teacher. First of all, I thank my parents for the patience, support and trust I enjoyed. I thank my children, Mihaela and Ionuț, for their understanding and lenience, and because they are my source of inspiration in everything I do. I also thank my husband for his support and kind words of encouragement.

Finally, I cannot end without thanking my collaborators at the high school where I work as a teacher for their help and constant encouragement.

Tremendously respectful,
Adina-Maria Păun

# INTRODUCTION

In recent decades, the intensification of human activities in various fields such as industry, agriculture, transport, etc. has led to a significant increase in the amount of organic and inorganic pollutants (especially heavy metals) released into the environment. Due to their toxicity, bioaccumulation potential and low clearance rate in the body, heavy metal and metalloid ions such as $Pb^{2+}$, $Hg^{2+}$, $Cd^{2+}$, $As^{3+}$, $As^{5+}$, $Cu^{2+}$ represent a threat to living organisms, endangering human health [1, 2]. The displacement of trace elements from their sites by heavy metal ions represents a major danger as it prevents the normal biological activity of enzymes and proteins [3]. Therefore, the detection and monitoring of these elements with toxic potential in different environments (soil, water, food, biological samples, etc.) require sensitive, fast and precise techniques. The classical analytical techniques used for the determination of heavy metal traces in various environmental samples such as atomic absorption spectrometry (AAS) [4], inductively coupled plasma mass spectrometry (ICP-MS) [5], flame atomic emission spectrometry (AES) [6], cold vapor atomic absorption spectrometry (CV-AAS) [7] are very efficient, but require well-controlled experimental conditions, laborious sample preparation and specialized personnel to perform the analyses [8].

An alternative to classical analytical techniques is represented by voltammetric techniques, namely anodic stripping voltammetry (ASV) which allows for the electrochemical detection of heavy metal traces in contaminated samples. The electrochemical sensors based on chemically modified electrodes exhibit increased sensitivity, selectivity, low cost, portability, and a fast response [9 - 11]. Their incorporation into portable devices allows for field monitoring of heavy metal ion concentrations in polluted areas.

The PhD thesis entitled: **CHEMICALLY MODIFIED ELECTRODES WITH APPLICATIONS IN THE CONTROL OF SOIL AND PLANT POLLUTION WITH INORGANIC POLLUTANTS IN THE SLATINA INDUSTRIAL AREA** addressed research areas aimed at the application of electrochemical techniques for the detection and monitoring of heavy metals in the environment and their combination with phytoremediation techniques that use plants for the remediation of polluted soil. The research topic of this work was a concern of the group of researchers in the laboratory of Electrochemical Processes in Organic Solvents (*EPOS*) from the Inorganic Chemistry, Physical Chemistry and Electrochemistry Department of the Faculty of Chemical Engineering and Biotechnology of the POLITEHNICA University in Bucharest. The research carried out by the researchers of the *EPOS* group aims to obtain new electrochemical sensors based on azulene and non-azulene derivatives.

The PhD thesis makes important contributions to the development of the current base of electrochemical sensors through the study of new azulene derivatives with properties of heavy metal ion complexation. All the electrochemical experiments carried out during the doctoral internship were performed using the existing material base in the *EPOS* laboratory. During the doctoral internship, several ligands were tested for the characterization of the CMEs surface for the molecular recognition of heavy metal ions. The studied ligands were synthesized by the researchers of the *C. D. Nenițescu* Center for Organic Chemistry - Romanian Academy. The best results obtained in the research activity carried out during the doctoral internship were published in 5 scientific papers: 1 article in the *Chemistry Journal* indexed BDI - co-author in 2020, 1 article in the *Journal of Electrochemical Science and Engineering* indexed Q3 - co-author in 2020, 1

article in the *Symmetry* magazine - author (IF = 2,645) in 2021, 1 article in the *Scientific Bulletin University Politehnica of Bucharest* - author in 2022, 1 article in the *Symmetry* magazine - co-author (IF = 2,940) in 2022 and 8 scientific paper sessions in poster form (7, 4 of which as author and 3 as co-author) and oral form (1 as co-author) at international conferences during the period between 2019 and 2022.

The PhD thesis presents elements of originality aimed at the electrochemical study of a new azulene-tetrazole derivative, E-5-((5-isopropyl-3,8-dimethylazulen-1-yl)diazenyl)-1H-tetrazole (**L**), which showed good results in the molecular recognition of heavy metal ions. The complexation properties of the new azulenic derivative were investigated by anodic stripping voltammetry and UV-Vis spectrophotometry. The obtained results showed that the ligand **L** in solution complexes the Pb (II) and Hg (II) ions, and that the chemically modified electrodes with poly**L** (**L**-CMEs) selectively complex the Pb (II) ion. These properties of ligand **L** have been exploited to obtain new electrochemical and spectrophotometric sensors with applications in the detection of heavy metal ions at low concentrations. The results of this study are presented in Chapter 4 of the thesis and were published in the *Symmetry* magazine.

The systematic studies carried out to improve the performances of the ligand **L**-based CMEs for heavy metal detection are presented in Chapter 5 of the thesis. Establishing the optimal parameters for the preparation of poly**L** films was achieved by testing several charge and potential values. The **L**-CMEs prepared by CPE in **L** (1 mM) solution at the potential of 0.5 V and the charge of 2 mC showed the best response for the analysis of the Pb (II) ion in mixed solutions of metal ions (Cu (II), Pb (II), Cd (II) and Hg (II)) of different concentrations ($10^{-8}$ M - $10^{-5}$ M), the detection limit being $10^{-8}$ M approximately. Through SEM and AFM experiments it was shown that the poly**L** films deposited on the surface show columnar formations, the roughness of the polymer surface (RMS) having the highest values at the potential of 0.5 V and the charge density of 28 mC/ $cm^2$ (corresponding to a charge of 2 mC). The research carried out in this chapter was published in the *University Politehnica of Bucharest Scientific Bulletin.*

A newly synthesized derivative based on azulen-thiophene-vinyl pyridine, namely 4-(azulen-1-yl)-2,6-bis((E)-2-(thiophen-2-yl)vinyl)pyridine (**M**), was investigated in order to obtain CMEs with applications in the detection of heavy metal traces in different samples, and the research results are presented in Chapter 6. The originality of the research consisted in the characterization of the poly**M** film surface prepared from **M** in different ways by SEM, AFM, FTIR and fluorescence methods. The morphology of the poly**M** film surface was correlated with the electrochemical properties of the **M** monomer in order to establish the application fields of **M**-based CMEs. The research results in this chapter were published in the *Symmetry* magazine.

In Chapter 7 of the PhD thesis, a statistical analysis of the experimental results obtained on soil and plant samples taken from the area of the aluminum plant in Slatina between 2011 - 2012 and 2019 is carried out based on parametric and non-parametric statistical tests. The exploratory analysis of each data set was performed by representing the boxplot diagrams, and the formal statistical analysis was performed by applying the parametric Two-Sample T-Test and the non-parametric Kruskal-Wallis H-Test and Dunnett's Test. The non-parametric statistical tests applied showed statistically significant differences ($p<0.05$) between the median concentrations of the Cu, Ni, Pb and Zn toxic potential elements in the 4 analyzed soils. The statistical studies carried out indicated a decrease in toxic element soil pollution in 2019 compared to the 2011 - 2012 period, which may be associated with a decrease in the plant oxidative stress caused by the presence of heavy metals. Further studies are needed to validate the results of this research.

The PhD thesis comprises 7 chapters arranged in two parts: PART I - **BIBLIOGRAPHY RESEARCH** and PART II - **ORIGINAL CONTRIBUTIONS**.

**THE BIBLIOGRAPHY RESEARCH** includes 3 chapters and presents the current level of knowledge concerning the most important aspects in specialized literature that refer to heavy metal soil pollution in the Slatina industrial area, the effects of pollution on plant and animal organisms, as well as methods of phyto/ mycoremediation of the polluted soil in the studied area. Chapter 3 presents a synthesis of the most recent studies on electrodes chemically modified with azulene derivatives and their use in the design of electrochemical sensors with applications in heavy metal detection and monitoring.

**CHAPTER 1. SOIL POLLUTION BY HEAVY METALS**

**CHAPTER 2. PLANT OXIDATIVE STRESS PRODUCED BY HEAVY METALS**

**CHAPTER 3. CHEMICALLY MODIFIED ELECTRODES. APPLICATIONS IN THE DETECTION OF HEAVY METAL IONS**

**The ORIGINAL CONTRIBUTIONS** include 4 chapters and consist of a detailed presentation of the original results obtained for the PhD thesis as well as their interpretation.

**CHAPTER 4. ELECTROCHEMICAL STUDY OF THE AZULENE-TETRAZOLIC DERIVATIVE E-5-((5-ISOPROPYL-3,8-DIMETHYLAZULEN-1-YL)DIAZENYL)-1H-TETRAZOLE (L) AND HEAVY METAL RECOGNITION BY USING CHEMICALLY MODIFIED ELECTRODES WITH POLYL**

**CHAPTER 5. STUDY TO IMPROVE THE PERFORMANCE OF NEW CHEMICALLY MODIFIED ELECTRODES WITH THE AZULENE DERIVATIVE L PREPARED FOR HEAVY METAL ION ANALYSIS**

**CHAPTER 6. CHARACTERISATION OF THE SURFACE OF CHEMICALLY MODIFIED ELECTRODES WITH LIGAND 4-(AZULEN-1-YL)-2,6-BIS((E)-2-(THIOPHEN-2-YL)VINYL)PYRIDINE (M)**

**CHAPTER 7. THE PROCESSING OF EXPERIMENTAL DATA OBTAINED ON SOIL AND PLANT SAMPLES BY STATISTICAL METHODS**

The PhD thesis ends with a chapter consisting of **GENERAL CONCLUSIONS,** which presents the main conclusions resulting from the study carried out in each chapter, **ORIGINAL CONTRIBUTIONS** and **PROSPECTS FOR FURTHER DEVELOPMENT** aimed at making proposals for the continuation of the study in the field. The work also contains tables and figures containing original data that represent the author's contribution.

The bibliography references, the list of articles published in scientific journals and the scientific papers presented at conferences, as well as the articles published *in extenso*, are attached.

# II. ORIGINAL CONTRIBUTIONS

# CHAPTER 4

# ELECTROCHEMICAL STUDY OF THE AZULENE-TETRAZOLIC DERIVATIVE E-5-((5-ISOPROPYL-3,8-DIMETHYLAZULEN-1-YL) DIAZENYL)-1H-TETRAZOLE (L) AND HEAVY METAL RECOGNITION BY USING CHEMICALLY MODIFIED ELECTRODES WITH POLYL

## 4.1. MOTIVATION FOR THE ELECTROCHEMICAL STUDY OF SOME AZULENIC DERIVATIVES FOR THE PRODUCTION OF CHEMICALLY MODIFIED ELECTRODES

The electrochemical study of some azulene derivatives was carried out in order to evaluate the possibility of obtaining CMEs used for heavy metal recognition.

This chapter presents the studies carried out during the doctoral internship by using a newly synthesized azulene-tetrazole derivative, E-5-((5-isopropyl-3,8-dimethylazulen-1-yl)diazenyl)-1H-tetrazole, denoted by **L** (Fig. 4.1) to prepare polymer films on the glassy carbon (GC) electrode and test their ability to complex heavy metals.

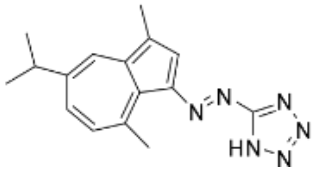


**Fig. 4.1.** The chemical structure of the azulene-tetrazole derivative **L**.

It can be seen that the azulene-tetrazole **L** derivative presented above and subjected to study has a polymerizable unit (the azulene derivative) and a metal ion complexation unit (in this case, the azotetrazole) in its structure, characteristics that were able to be used for the electrooxidative polymerization of ligand **L**, coupled with the molecular recognition of heavy metal ions (Pb (II), Cd (II), Cu (II), Hg (II)).

The study of ligand **L** started with its electrochemical characterization which was carried out using the following voltammetric methods: Cyclic Voltammetry - CV, differential pulse voltammetry - DPV and Rotating Disk Electrode Voltammetry - RDE. The conditions for obtaining complexing polymer films deposited on GC were established. The recognition method was based on the stripping analysis of the electrodes modified with poly**L** films (**L**-CMEs) using the DPV technique available in the potentiostat software.

## 4.2. MATERIALS AND APPARATUS

The synthesis of the azulene derivative **L**, whose chemical structure is shown in Fig. 4.1, was performed according to the methodology described in the reference [4.15]. In the voltammetric experiments performed, tetrabutylammonium perchlorate (TBAP, from Fluka, Munich, Germany, purity ≥ 99%) was used as supporting electrolyte, and acetonitrile ($CH_3CN$, from Sigma Aldrich,

99.999% purity) as solvent. A 0.1 M acetate solution (pH = 4.5) was used as a buffer solution, prepared from 0.2 M acetic acid solutions (Fluka, >99%), 0.2 M sodium acetate (Riedel de Haën, Seelze, Germany) and ultrapure water. Stock solutions of heavy metal salts of $10^{-3}$ M concentration were prepared by dissolving the salts of mercury (II) acetate (Sigma Aldrich), dihydrate cadmium (II) acetate (Fluka, ≥98%), trihydrate (II) lead acetate (Fluka, ≥99.5%) and monohydrate (II) copper acetate (Fluka, ≥98%) in ultrapure water. Working solutions of metal ion salts with concentrations between $10^{-4}$ M and $10^{-8}$ M were prepared from the stock solutions of $10^{-3}$ M concentration by dilution.

A three-electrode cell connected to an AUTOLAB PGSTAT 302 N potentiostat was used for the electrochemical experiments (Fig. 4.2). The working electrode of the cell was a glassy carbon disc (d = 3 mm, Metrohm, Herisau, Switzerland), the reference electrode used was an Ag electrode/ 10 mM $AgNO_3$, 0.1 M TBAP/ $CH_3CN$, and the counter electrode was a Pt wire. The potentials were reported to the reversible ferrocene/ ferricinium ($Fc/ Fc^+$) system. At the beginning of each experiment, the surface of the glassy carbon electrode was polished by diamond paste (2 μm) on electrode felt, and the excess diamond paste on the electrode surface was removed by rinsing with acetonitrile.

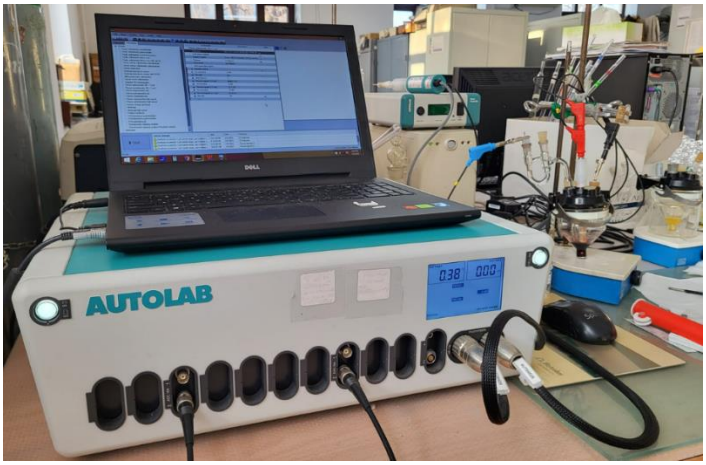


**Fig. 4.2.** AUTOLAB PGSTAT 302 N potentiostat connected to the electrochemical cell containing the ligand **L** solution.

The CV curves were recorded at a scan rate of 0.1 V/ s or at different potential scan rates in the range of 0.1 - 1 V/ s, to study the influence of this parameter. The curves obtained by DPV were recorded for the scan rate of 0.01 V/ s with a pulse height of 0.025 V and a time interval of 0.2 s. The RDE curves were recorded at a scan rate of 0.01 V/ s using different electrode rotation rates, namely 500, 1000 and 1500 rpm. For heavy metal cation recognition experiments using the obtained CMEs, the reference electrode was Ag/ AgCl, 3M KCl, $H_2O$, and the counter electrode was a Pt wire.

**L**-CMEs were prepared in solutions of ligand **L** of 1 mM concentration in 0.1 M TBAP/ $CH_3CN$. After preparation, each CME was taken out of the solution, equilibrated and overoxidized in 0.1 M acetate buffer solution (pH = 4.5), following the methodology described in references [4.16] and [4.17]. Then, it was immersed for 15 minutes under controlled stirring in a solution of heavy metal ions (Cu (II), Pb (II), Cd (II), Hg (II)) of different concentrations: $10^{-8}$ M, $10^{-7}$ M, $10^{-6}$ M, $10^{-5}$ M and $10^{-4}$ M. The **L**-CME complexed with metal ions was removed from the storage solution, rinsed with distilled water and introduced into the analysis cell containing a buffer

solution of 0.1 M acetate (pH = 4.5). Here the electrode was polarized for 3 min at -1.2 V, and anodic redissolution curves were recorded between -1.2 V and +0.8 V.

## 4.3. ELECTROCHEMICAL STUDY OF LIGAND **L**

The electrochemical behavior of ligand **L** was studied by three voltammetric methods: DPV, CV and RDE. Figure 4.5 shows the DPV and CV curves recorded during **L** oxidation and reduction for different concentrations in 0.1M TBAP/ $CH_3CN$ supporting electrolyte. The DPV curves illustrated in Fig. 4.5A show two main anodic peaks for **L**, denoted a1 and a2, and three secondary peaks, a3, a4 and a5, which overlap the oxidation range of the solvent. In the cathodic scan, five cathodic peaks are observed, denoted c1, c2, c3, c4 and c5, of which the largest (in absolute value) are c1, c2 and c3. The peak corresponding to c1 in the return scan was denoted c1'. The CV curves illustrated in Fig. 4.5B show two oxidation peaks corresponding to peaks a1 and a2 in DPV, and a broad peak over the potential domain covering peaks a3 - a5 in DPV. In the cathodic scan, five peaks are observed in the CV in good agreement with peaks c1 - c5 in the DPV. The anodic and cathodic peak currents in the CV and DPV curves increase with the concentration of ligand **L**. The other smaller signals at negative potentials (-1.2 V – -1.4 V) are attributed to the reduction of oxygen traces in the residual water, as a secondary process ($O_2$/ $O_2$−).

Figure 4.6A shows the CV curves obtained at different scan rates (V/ s) recorded in **L** solution (1 mM), when scanning in the potential range of the anodic peak a1 and the cathodic peak c1. All peak currents increase when increasing scan rate. The appearance of a cathodic peak c1' corresponding to the return scan was observed, which attests to the fact that c1 is a quasi-reversible process.

To verify the diffusion character of the electrode processes, the graph of the peak current (ip) was drawn as a function of the square root of the scan rate ($v^{1/2}$) for the anodic (a1) and cathodic (c1) peaks, dependencies shown in Fig. 4.6B. The linear dependence of the peak currents (ip) on the square root of the scan rate ($v^{1/2}$) can be observed, according to equations (4.1) and (4.2) below:

$$ipa1\ (\mu A) = 1{,}00 + 60 \cdot v^{1/2}\ (R^2 = 0{,}997) \quad (4.1)$$

$$ipc1\ (\mu A) = 8{,}05 - 95 \cdot v^{1/2}\ (R^2 = 0{,}994) \quad (4.2)$$

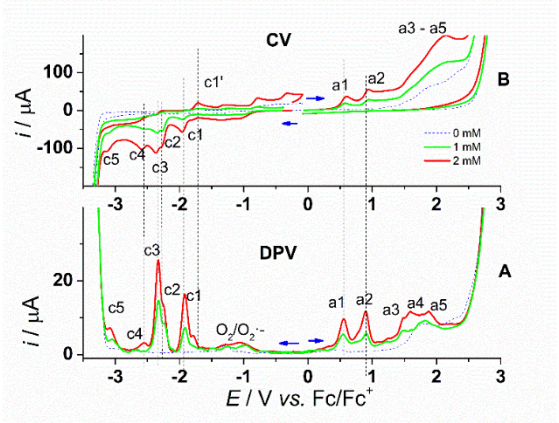


**Fig. 4.5.** DPV curves (**A**) and CV curves (**B**) recorded at 0.1 V/ s on glassy carbon electrode for **L** in 0.1 M TBAP/ $CH_3CN$ at different concentrations: 0 (dotted blue line), 1 mM (green line ), 2 mM (red line). DPV currents are shown in absolute value.

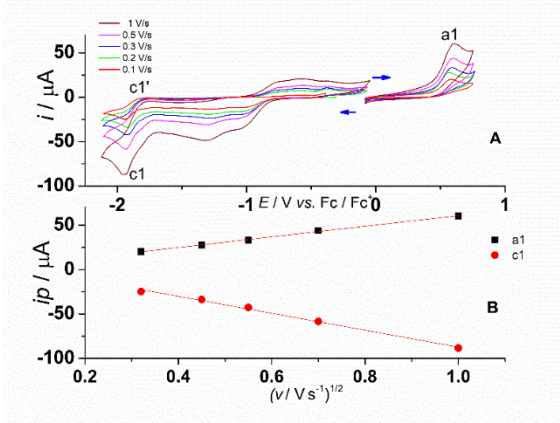


**Fig. 4.6.** CV voltammetric curves on glassy carbon electrode in 1 mM **L** solution in 0.1 M TBAP/ $CH_3CN$ at different scan rates (**A**); dependence of the peak current on the square root of the scan rate for peaks a1 and c1 (**B**).

The values of the peak potentials from the CV and DPV curves measured for the **L** solution (1 mM), but also the characteristics of the processes are presented in Table 4.1.

**Table 4.1. Values of anodic (a) and cathodic (c) peak potentials (in V) from CV and DPV curves, half-wave potential ($E_{1/2}$) from RDE for L (1 mM) and associated process characteristics obtained from CV curves over different domains and scan rates.**

| Peak | Method | | | Process characteristics |
|---|---|---|---|---|
| | CV | DPV | RDE ($E_{1/2}$) | |
| a1 | 0,57 | 0,55 | | Irreversible |
| a2 | 0,93 | 0,90 | | Quasi-reversible |
| c1 | -1,95 | -1,91 | -1,867 (500 rpm)<br>-1,888 (1000 rpm)<br>-1,906 (1500 rpm) | Quasi-reversible |
| c1’ | -1,70 | | | - |
| c2 | -2,26 | -2,23 | | Irreversible |
| c3 | -2,34 | -2,32 | -2,288 (500 rpm)<br>-2,292 (1000 rpm)<br>-2,330 (1500 rpm) | Quasi-reversible |
| c4 | -2,57 | -2,55 | | Quasi-reversible |
| c5 | -3,11 | -3,05 | | Irreversible |

Figure 4.8 compares the RDE curves (at the bottom, labeled A) at different rotation rates for **L** (1 mM) and the corresponding anodic and cathodic DPV curves (at the top, labeled B). The anodic RDE curves show a single wave corresponding to the a1 peak potential in DPV. The cathodic RDE curves show two clear waves, denoted w1 and w2, corresponding to peaks c1 and c2 - c3, respectively, in DPV (which are located at too-close potentials to be separated in RDE, but distinguishable in DPV). Increasing the rate of rotation of the electrode leads to an increase in the limiting currents of the cathodic waves. The limiting current of the anodic wave in RDE decreases when the electrode rotation rate increases. It can be observed that at potentials more positive than those for the a2 peak in DPV, the current drops suddenly. The same behavior was observed in other cases of azulene derivatives when the electrode was covered with a polymer film [4.12]. The half-wave potential values in RDE for the cathodic processes shown in Table 4.1 are consistent with the peak potential values obtained by the DPV and CV methods.

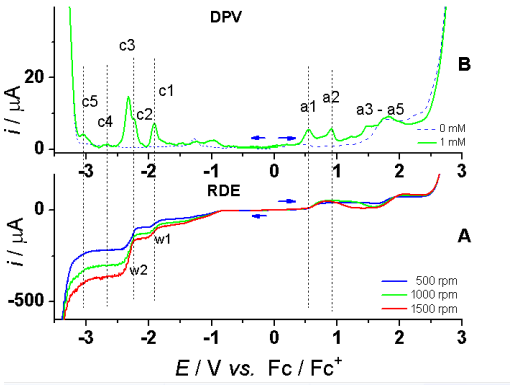


**Fig. 4.8.** RDE curves at different rotation rates (rpm) (**A**) and DPV curves (**B**) on glassy carbon electrode for the **L** (1 mM) solution. DPV currents are shown in absolute value.

## 4.4. OBTAINING CHEMICALLY MODIFIED ELECTRODES WITH POLY**L**

The GC electrodes were modified with poly**L** films in 1 mM **L** solution in 0.1 M TBAP/ $CH_3CN$ by successive potential cycling with an anodic limit located in the range of peaks a1 and a2 (0.75 V, 1 V) or by controlled potential electrolysis (CPE) using different charges and potentials, namely 1 mC, 0.75 V/ 1 V, 2 mC, 1 V. As observed in Fig. 4.9, the peak current for a2 decreases in successive cycles, especially when the potential is scanned in the range of the a2 peak. This is evidence of the electrode being coated with polymer film, the coating being confirmed by transfer to the 1 mM ferrocene solution in 0.1 M TBAP/ $CH_3CN$ when the cyclic voltammograms shown in Fig. 4.10A were recorded. Figure 4.10B shows the CV curves recorded after the transfer into ferrocene solution for the **L**-CMEs prepared by CPE at different charges and potentials. It can be seen that the ferrocene signal for the poly**L** film modified electrode prepared by successive cycling or CPE is slightly shifted in anodic and cathodic peak potential, and that the peak currents remain practically the same. This fact suggests the formation of thin, porous films.

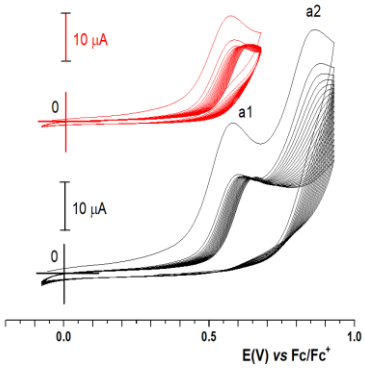


**Fig. 4.9.** CV curves (0.1 V/s) recorded during the preparation of **L**-CMEs by cycling the potential (20 cycles) with the anodic limit in the range of peaks a1 and a2.

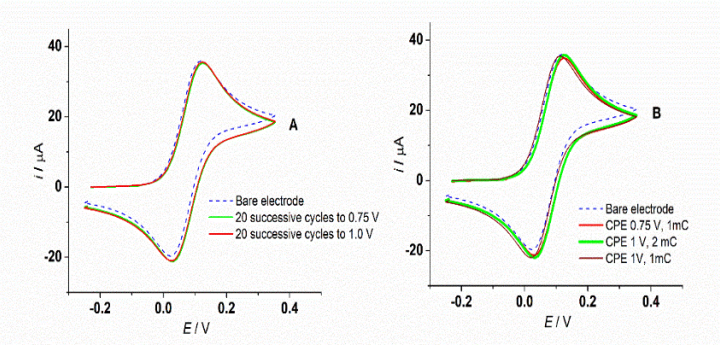


**Fig. 4.10.** CV curves (0.1 V/s) recorded by transfer in 1 mM ferrocene solution for **L**-CMEs prepared by potential cycling (20 cycles) in the range of a1 and a2 peaks (**A**), and by CPE at: 0.75 V and 1 mC, 1 V and 2 mC, 1 V and 1 mC (**B**).

## 4.5. DETECTION OF HEAVY METAL IONS USING POLY**L**

For heavy metal recognition, **L**-CME was prepared by CPE in 1 mM **L** solution in 0.1 M TBAP/ $CH_3CN$ at 1 V potential and 1 mC charge, the parameters providing better GC coverage with thin film formation, as previously shown. The procedure used was the same as for other azulene derivatives [4.17]. Different concentrations of the storage solutions were tested in the following order: $10^{-8}$ M, $10^{-7}$ M, $10^{-6}$ M, $10^{-5}$ M, $10^{-4}$ M (for each cation). Anodic redissolution curves were recorded between -1.2 V and +0.8 V using the DPV method and are shown in Fig. 4.15. The DPV peak currents corresponding to each cation were read and the $i_{peak}$ *vs* $[Me^{2+}]$ graph was plotted (Fig. 4.16).

The stripping currents in the DPV curves decrease according to the concentration of the ions in the storage solution in the following order: Pb>Hg>Cu>Cd. The recognition peaks with the best response were obtained for Pb (II) and Hg (II) in the mixed accumulation solutions having concentrations of $10^{-5}$ M and $10^{-4}$ M, respectively, suggesting that the **L**-CMEs prepared by CPE at 1 V and 1 mC showed selective complexation for the two cations. According to the linearity of

the points in the $i_{peak}$ *vs* $[Pb^{2+}]$ graph (Fig. 4.17) in the range $10^{-8}$ M - $10^{-5}$ M ($R^2$ = 0.9752), it can be stated that **L**-CMEs can be used for the analysis of the wastewater Pb (II) ion at a detection limit of $10^{-8}$ M.

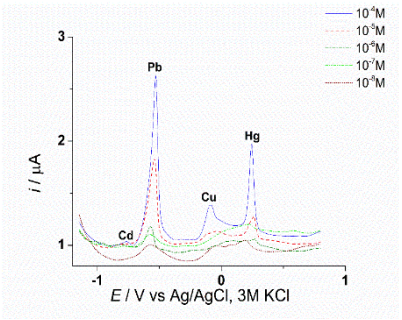


**Fig. 4.15.** DPV curves (0.01 V/s) recorded for **L**-CMEs prepared at +1 V and 1 mC after immersion in mixed metal ion storage solutions of different concentrations (M).

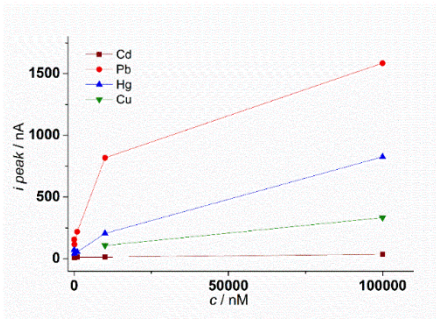


**Fig. 4.16.** Dependence of the peak currents in DPV for each metal on the metal ion concentration in the mixed storage solutions.

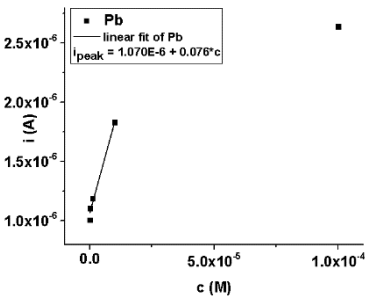


**Fig. 4.17.** Linear dependence of the peak current in DPV on the concentration of the Pb(II) ion in the range $10^{-8}$ M - $10^{-5}$ M.

## 4.6. STUDY OF THE COMPLEXATION PROPERTIES OF LIGAND E-5-((5-ISOPROPYL-3,8-DIMETHYLAZULEN-1-YL)DIAZENYL)-1H-TETRAZOLE BY UV-VIS SPECTROMETRY

The study of the complexation properties of the newly synthesized azulene-tetrazole derivative, E-5-((5-isopropyl-3,8-dimethylazulen-1-yl)diazenyl)-1H-tetrazole (**L**) was carried out by UV-Vis molecular absorption spectrometry.

### 4.6.1. UV-Vis study of Pb (II) ion complexation with ligand L

In order to follow the interaction mechanism of ligand **L** of concentration 7.06 µM in 0.1 M TBAP/ $CH_3CN$ with Pb (II) metal ions, its spectrophotometric titration was performed in the presence of the metal ion amounts in the molar ratios, by stirring the samples for 1 minute, and recording each spectrum in an 8-minute interval. Changes were found in the recorded spectra following the addition of increasing concentrations of Pb (II) solutions (a few µL of $10^{-3}$ M trihydrate lead (II) acetate in ultrapure water) to 3 mL of a 7.06 µM **L** solution in $CH_3CN$. In the UV-Vis spectra recorded and shown in Fig. 4.23 (picture on the left), when the [Pb(II)]/ [**L**] ratio increases, hypo, hyper and hypso-chromic shifts of all bands of **L** ligand are observed. The formation of the five isosbestic points (I1' = 451.3 nm, I2' = 383.9 nm, I3' = 347.7 nm, I4' = 324.7 nm, I5' = 271.2 nm) in the absorption spectra confirmed that during the titration process, both ligand **L** and its Pb (II) ion complexes can be found in the solution. In the calibration curve in Fig. 4.23 (picture on the right) as the molar ratio [Pb(II)]/ [**L**] increases, the absorbance of the maximum peak at 486 nm decreases. After adding a [Pb(II)]/ [**L**] molar ratio of 0.6/ 1, the absorbance values are practically constant, and a level that corresponds to a saturation stage where **L** was totally complexed with Pb (II) ions is reached.

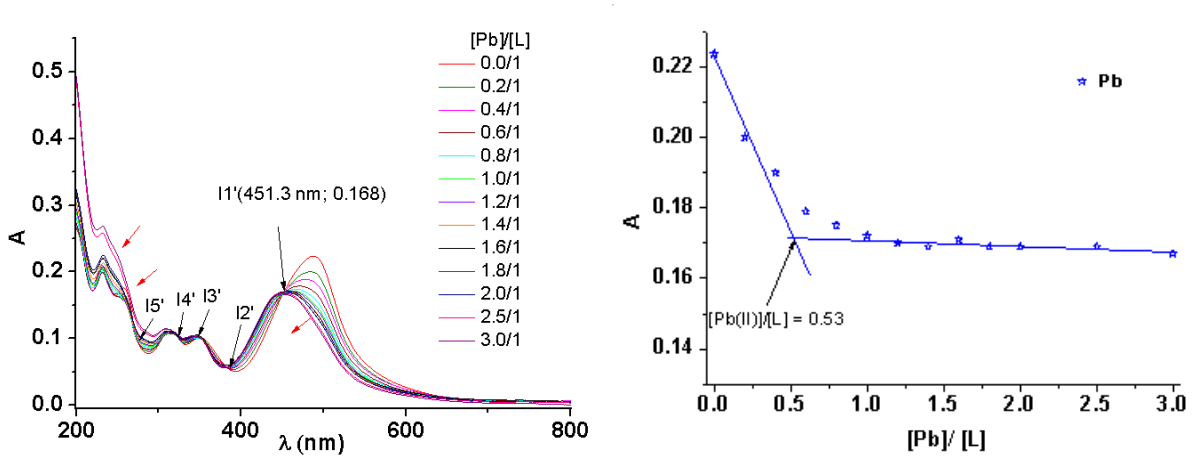


**Fig. 4.23.** Absorption spectra of ligand **L** complexes (7.06 μM in $CH_3CN$) with different amounts of Pb (II) ions in solution (left-hand picture); black arrows indicate isosbestic points, red arrows indicate the direction in which absorbance values move with increasing Pb (II) concentration; Maximum visible peak absorbance *vs* [Pb(II)]/ [**L**] ratio (right-hand picture), [**L**] ≈ constant.

### 4.6.2. UV-Vis study of Hg (II) ion complexation with ligand L

In order to study the interaction of ligand **L** with Hg (II) ions, the spectrophotometric titration of a 7.06 μM **L** solution in $CH_3CN$ was performed in the presence of metal ions in established molar ratios [Hg(II)]/ [**L**], the complexation time being of 1 minute. Figure 4.26 (picture on the left) shows that, by adding increasing concentrations of the Hg (II) solution (a few μL of $10^{-3}$ M mercuric (II) acetate in ultrapure water) to the ligand **L** solution, changes were found in the recorded spectra, all five absorption bands having undergone hypo and hypso-chromic shifts. The seven isosbestic points (I1 = 449 nm, I2 = 381.6 nm, I3 = 324.2 nm, I4 = 271.2 nm, I5 = 249.7 nm, I6 = 238.1 nm, I7 = 212 nm) identified in the absorption spectra confirmed the presence in solution of the uncomplexed ligand **L** and its Hg (II) ion complexes. In the calibration curve in Fig. 4.26 (picture on the right), increasing the molar ratio [Hg(II)]/ [**L**] initially results in a linear decrease in the absorbance of the maximum peak from 486 nm. After adding a [Hg(II)]/ [**L**] molar ratio of 0.6/ 1, a slow decrease in absorbance values is observed. The value of the molar ratio [Me(II)]/ [**L**] at the point where the slope of the line changes is equal to the Me(II)/ **L** ratio in the complex. Since [Pb(II)]/ [**L**] = 0.53 ≈ 1/ 2 and [Hg(II)]/ [**L**] = 0.61 ≈ 1/ 2, it follows that the probable formula of the complexes formed by the ligand **L** with the ions of Pb (II) and Hg (II) determined by the molar ratio method [4.19] is Me(II)$\mathbf{L}_2$.

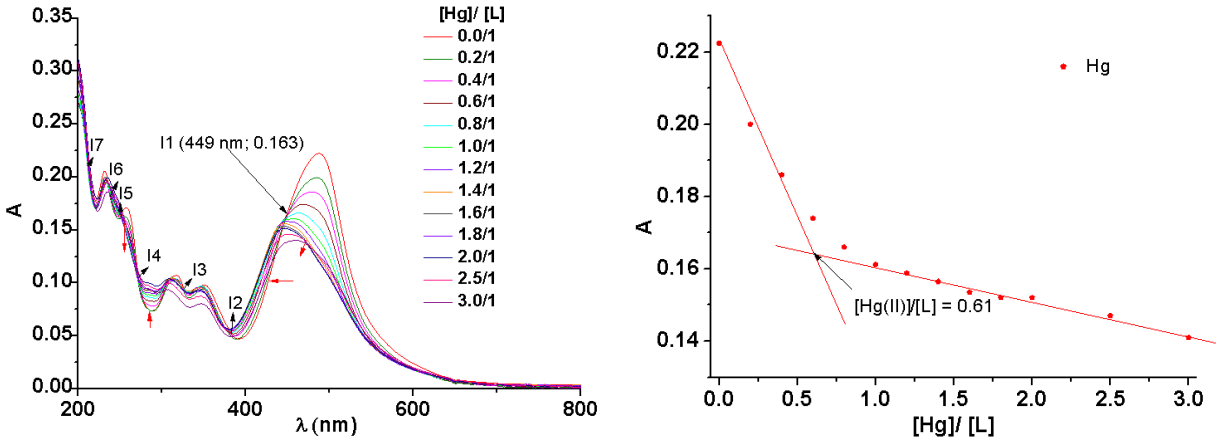


**Fig. 4.26.** Absorption spectra of ligand **L** complexes (7.06 μM in $CH_3CN$) with different amounts of Hg (II) ions in solution (left-hand picture); black arrows indicate isosbestic points, red arrows indicate the direction in which absorbance values move with increasing the Hg (II) concentration; Maximum visible peak absorbance *vs* [Hg(II)]/ [**L**] ratio (right-hand image), [**L**] ≈ constant.

# CHAPTER 5
# STUDY TO IMPROVE THE PERFORMANCE OF NEW CHEMICALLY MODIFIED ELECTRODES WITH THE AZULENE DERIVATIVE L PREPARED FOR HEAVY METAL ION ANALYSIS

This chapter presents the results obtained from the study carried out to improve the conditions of obtaining the **L** (**L**-CMEs) chemically modified electrodes, which were studied and presented in Chapter 4, in order to analyze HMs ions at low concentrations in water samples. The analytical performances of the **L**-CMEs prepared by CPE at different charges and potentials were tested for the analysis of HMs ions in mixed solutions of Cu (II), Pb (II), Cd (II), and Hg (II). The surfaces of the **L**-CMEs from which the best analytical signals were obtained were examined by scanning electron microscopy (SEM), atomic force microscopy (AFM) and micro-Raman spectroscopy to show the influence of CMEs preparation conditions on the characteristics of polymer films.

## 5.1.1. Materials and methods for HMs analysis

**L**-CMEs were obtained by CPE in solution of **L** (1 mM) in 0.1 M TBAP/ $CH_3CN$ at different charges and potentials for HMs analysis according to previously published procedure [5.2, 5.7].

## 5.1.2. Chronoamperometric curves recorded during L-CMEs preparation

In order to perform chronoamperometric experiments, the **L**-CMEs were prepared in solution of **L** (1 mM) in 0.1 M TBAP/ $CH_3CN$ by CPE at different charge densities and oxidation potentials located before the a1 peak (+0.5 V) and after the a2 peak in DPV (+1 V, +1.25 V, +1.5 V, +2.5 V), as seen in Table 5.1, according to the procedure described in specialized literature and in the case of other azulene derivatives [5.1, 5.2].

**Table 5.1. Preparation and test conditions of L-CMEs on GC (d = 3 mm), denoted by CME, or on GC (d = 6 mm), denoted by CMEp.**

| Sample | Applied potential in CPE (V) | Applied charge in CPE (mC) | Charge density in CPE ($mC/cm^2$) | Type of investigation |
|---|---|---|---|---|
| CME1a | 1 | 0,5 | 7,04 | HMs Analysis |
| CME1b* | 1 | 1 | 14,08 | Ferrocene redox probe (Fc), HMs analysis |
| CME1c | 1,25 | 1 | 14,08 | TBAP (CV in 0,1M TBAP/ $CH_3CN$) |
| CME1* | 1 | 2 | 28,16 | Fc** |
| CME2 | 1 | 3 | 42,25 | Fc |
| CME3 | 1 | 4 | 56,33 | Fc |
| CME3b | 1 | 6 | 84,48 | Fc, HMs analysis |
| CME4 | 0,5 | 0,5 | 7,04 | HMs analysis |
| CME5 | 0,5 | 1,790 | 25,21 | HMs analysis |
| CME6 | 0,5 | 1,741 | 24,52 | HMs analysis |
| CME7 | 0,5 | 2 | 28,16 | Fc |
| CME8 | 0,8 | 2 | 28,16 | Fc |
| CME9 | 0,5 | 2 | 28,16 | HMs analysis |
| CME10 | 0,5 | 2 | 28,16 | HMs analysis |
| CME11 | 0,5 | 1 | 14,08 | HMs analysis |
| CMEp12 | 2,5 | 4 | 14,08 | Scanning Electron Microscopy (SEM) |
| CMEp13 | 1,5 | 4 | 14,08 | SEM |
| CMEp14 | 1 | 4 | 14,08 | SEM |
| CMEp15 | 1 | 8 | 28,16 | SEM |
| CMEp16 | 1 | 24 | 84,48 | SEM |
| CMEp17 | 0,5 | 8 | 28,16 | SEM, Atomic Force Microscopy (AFM), micro-Raman Spectroscopy |
| CMEp18 | 0,5 | 7,4 | 26,05 | SEM, AFM, micro-Raman Spectroscopy |
| CMEp19 | 0,8 | 8 | 28,16 | SEM |

* presented in Chapter 4; ** Fc - Ferrocene.

Figures 5.1 and 5.2 show the chronoamperograms recorded on GC pellet electrodes (d = 6 mm) at different oxidation potentials (+0.5 V, +0.8 V, +1 V, +1.5 V and +2.5 V) and the same electropolymerization charge of 8 mC (Fig. 5.1) and 4 mC (Fig. 5.2). When the applied potential increases, the values of the chronoamperogram limit currents increase and the time required to reach a constant charge decreases.

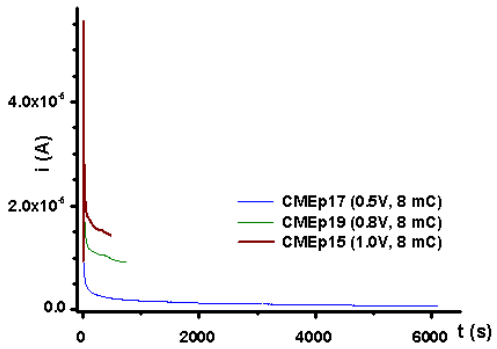


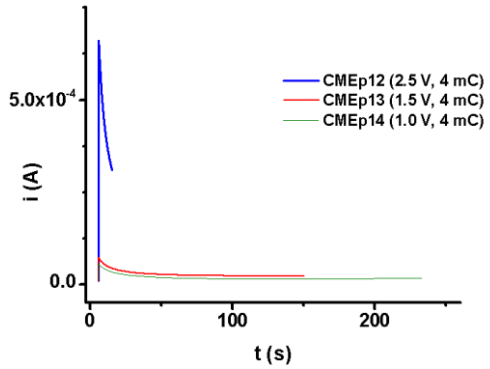

**Fig. 5.1.** Chronoamperograms recorded on GC pellet electrodes (d = 6 mm) obtained during the deposition of poly**L** films; polymer films were prepared by CPE at the same charge of 8 mC and different potentials (+0.5, +0.8, +1 V).

**Fig. 5.2.** Chronoamperograms recorded on GC pellet electrodes (d = 6 mm) obtained during the deposition of poly**L** films; polymer films were prepared by CPE at the same charge of 4 mC and different potentials (+1, +1.5, +2.5 V).

### 5.1.3. Highlighting the formation of films on L-CMEs by transfer in ferrocene and TBAP support electrolyte

The CV curves in Fig. 5.5, recorded after the transfer of **L**-CMEs in the 0.1 M TBAP/ $CH_3CN$ electrolyte solution showed higher hysteresis than those obtained on the bare GC electrode, both for **L**-CMEs prepared by CPE at 1.25 V and 1 mC, as well as for those obtained by successive cycling of the potential between -0.5 V and +1.25 V (5 cycles). The presence of the polymer film deposited on the GC can also be highlighted by the appearance of an anodic shoulder at approximately 0 V and of a cathodic peak at about -0.1 V. The values of these potentials were also found when preparing the polymer film by potential scanning, as can be seen in Fig. 5.5.

Figure 5.6A shows the influence of the potential applied in the CPE during the preparation of the films on the chronoamperometric curves. **L**-CME transfer in 1 mM ferrocene solution in 0.1 M TBAP/ $CH_3CN$ obtained at 0.5 V and 2 mC with a film deposition time of about 8800 s shows a highly modified CV curve compared to that recorded on the bare GC electrode. By comparison, **L**-CME prepared at 0.8 V and 2 mC with a film deposition time of 280 s has a ferrocene signal very close to that on the bare GC electrode, as seen in Fig. 5.6B. Following the chronoamperograms in Fig. 5.6A, it can be said that, at a potential of 0.5 V, the current values are small and the polymerization is slow, but the film deposition time on the electrode is sufficient; at the potential of 0.8 V, the current values are high, but there is about 31 times less time for film deposition (8800/ 280 ~ 31). For the **L**-CME prepared at the potential of 0.8 V, the decrease in current for ferrocene is insignificant, the ferrocene formal potential (Ef = (Epa + Epc)/ 2) is slightly shifted, and the potential difference between the anodic peak and the cathodic peak ($\Delta Ep = Epa - Epc$) increases slightly, as shown in Fig. 5.6B. This behavior could be explained as follows: the disturbed ferrocene signal for the CME prepared at the potential of 0.5 V (corresponding to the peak value for a1) and the charge of 2 mC (CME7) indicates a better coverage of the GC electrode with a film polymer which has different structure and properties from the polymer film deposited on the GC at the potential of 0.8 V and the same charge (CME8).

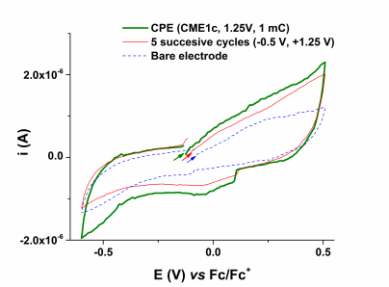


**Fig. 5.5.** CV curves (50 mV/s) recorded after **L**-CMEs transfer in 0.1 M TBAP/ $CH_3CN$ supporting electrolyte and on the bare GC electrode; **L**-CMEs were obtained in 1 mM **L** solution in 0.1 M TBAP/ $CH_3CN$ by successive cycling (5 cycles) (50 mV/s) between -0.5 V and +1.25 V and by CPE at +1.25 V and 1 mC.

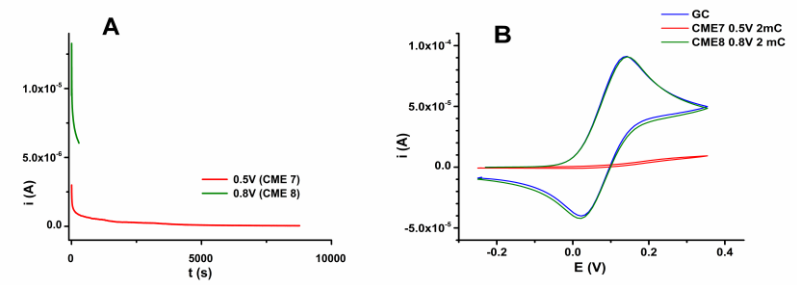


**Fig. 5.6.** Chronoamperograms recorded during the preparation of poly**L** films (**A**) and the corresponding CV curves (0.05 V/s) after **L**-CMEs transfer in 1 mM ferrocene solution in 0.1 M TBAP/ $CH_3CN$ compared to those recorded on the bare GC electrode (**B**); **L**-CMEs were prepared at different potentials (using the same 2 mC charge): +0.5 V (about 8800 s) and +0.8 V (280 s).

The CV curves in Figure 5.7B recorded after **L**-CMEs transfer in 1 mM solution of ferrocene in 0.1 M TBAP/ $CH_3CN$ show that, as the charge used in electropolymerization increases (1, 2, 3, 4, 6 mC) at a constant potential (1 V), the intensity of the ferrocene signal does not change significantly. The shape of the CV curves can be explained by following the chronoamperograms in Fig. 5.7A obtained during the preparation of poly**L** films and showing the correlation between the charge used and the film deposition time. The ferrocene/ ferricinium system has a similar value of about 100 mV for ΔEp on the CMEs and the bare GC electrode, suggesting the formation of thin/ porous films.

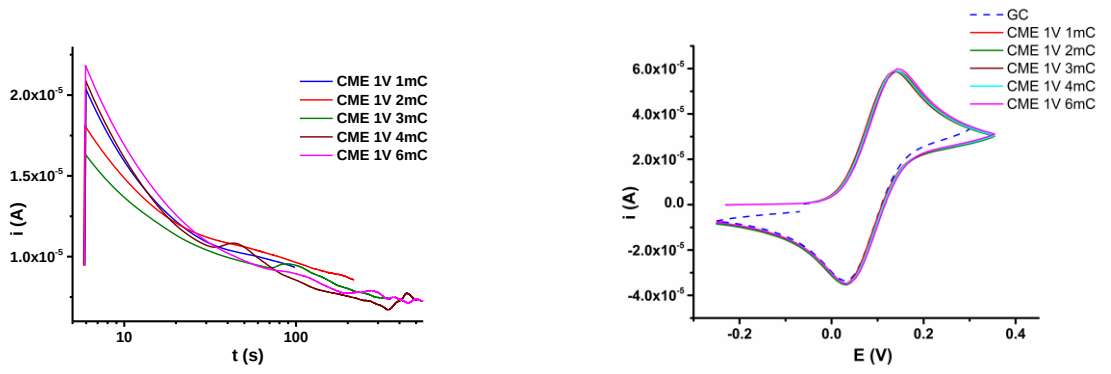


**Fig. 5.7.** Chronoamperograms recorded during the preparation of poly**L** films (**A**) and the corresponding CV curves (0.1 V/s) after **L**-CMEs transfer in 1 mM ferrocene solution in 0.1 M TBAP/ $CH_3CN$ compared to those recorded on the bare GC electrode (**B**); **L**-CMEs were prepared by CPE at +1 V and different charges (1, 2, 3, 4, 6 mC).

### 5.1.4. Analysis of heavy metals (Cd, Pb, Cu, Hg) using the new L-CMEs

The properties of heavy metal cation complexation of **L**-CMEs prepared by CPE in **L** solution (1 mM) at different charges and potentials were investigated using the open circuit chemical preconcentration method paired with the anodic stripping technique. The influence of different parameters (preparation potential and charge density in CPE) was studied to improve the **L**-CMEs performance in the analysis of HMs.

Figures 5.9 and 5.10 show the stripping DPV curves for **L**-CMEs prepared by CPE at different charges and potentials in **L** solution (1 mM) in 0.1 M TBAP/ $CH_3CN$, after immersion in mixed HMs storage solutions of $10^{-6}$ M and $10^{-5}$ M (of each investigated cation).

Figures 5.9A and 5.9B show the DPV curves for the films prepared at 0.5 V and different charges (0.5 mC, 1 mC, 1.79 mC), and the dependence of the peak currents in the DPV on the electrical charge used in CPE, respectively. Figure 5.9B shows a linear increase in DPV peak currents for Pb ($\Delta i_{peak\ Pb}$) at the same time as the electrical charge, the slope of the line being $4.66 \cdot 10^{-7}$ A/ mC ($\Delta i_{peak\ Pb}$ = -9.89E-8 + 4.66E -7·q). The same linear dependence was observed for the Pb peak surface ($\Delta A_{peak\ Pb}$). This also proves that the film is porous because the linear dependence shows that metal ions can penetrate the films in a similar manner, regardless of their thickness (a thicker film gives a better signal), which is a very good feature of the film and therefore of the **L**-CMEs. Their chronoamperograms as well as the corresponding CV curves in the ferrocene probe solution indicate that reproducible films were formed.

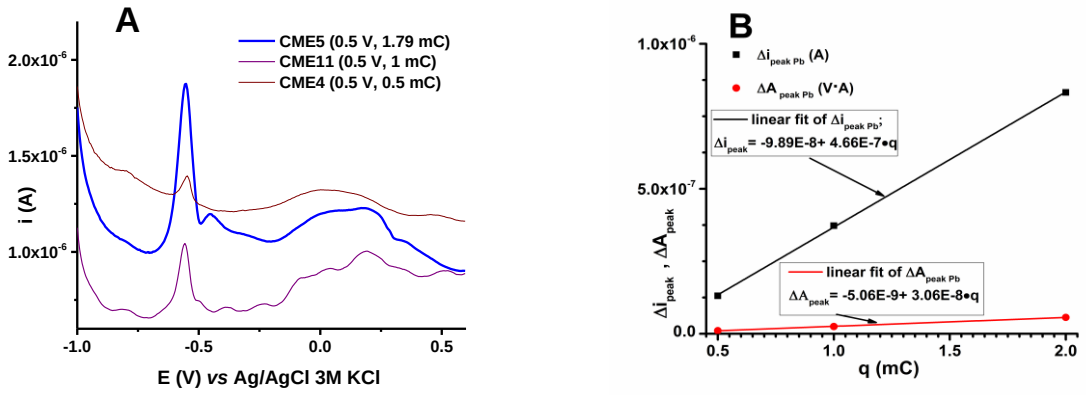


**Fig. 5.9.** Stripping DPV curves (0.01 V/ s) for **L**-CMEs conditioned and immersed in mixed metal ion accumulation solutions (Cd (II), Pb (II), Cu (II) and Hg (II)) ($10^{-6}$ M for each cation) (**A**) and the dependence of the peak current in DPV ($\Delta i_{peak\ Pb}$) and the peak area ($\Delta A_{peak\ Pb}$) on the q charge applied in CPE (**B**); **L**-CMEs were prepared at +0.5 V and different charges (0.5, 1, 1.79 mC).

Figure 5.10 confirms the influence of the electric charge on the analytical signals of all cations in the synthesis performed by CPE at 1 V and 84 mC/ $cm^2$. Increasing charge results in an increase in analytical signals for all metal ions, with slopes expressed in A/ mC of $0.4 \cdot 10^{-7}$ (Cd), $1.84 \cdot 10^{-7}$ (Pb), $0.116 \cdot 10^{-7}$ (Cu) and $0.98 \cdot 10^{-7}$ (Hg). It is observed that the slope obtained for Pb at 1 V ($1.84 \cdot 10^{-7}$) is lower than the one obtained at 0.5 V ($4.66 \cdot 10^{-7}$), although the film is thicker. This shows that the analytically optimal synthesis potential is 0.5 V. Increasing the film thickness results in an intensification of the signal.

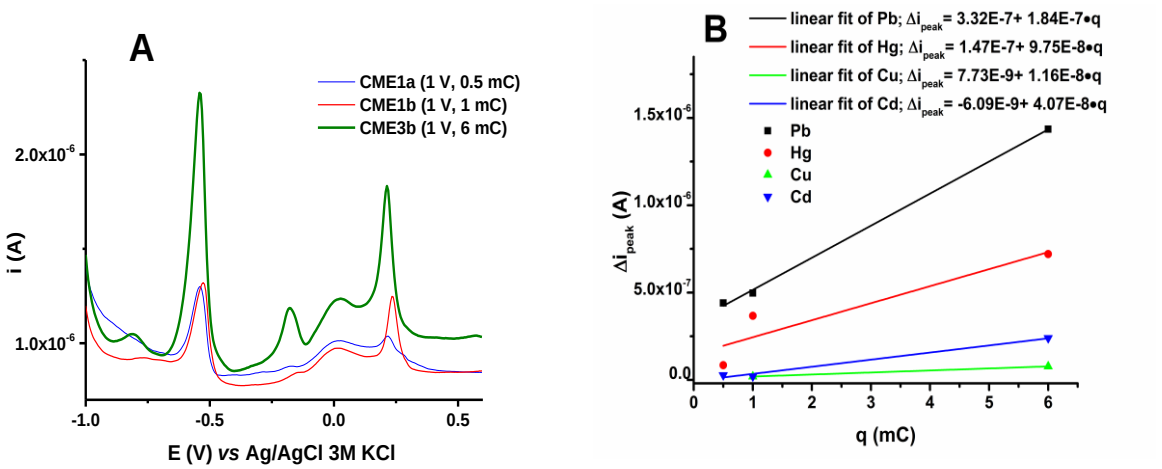


**Fig. 5.10.** Stripping DPV curves (0.01 V/ s) for **L**-CMEs conditioned and immersed in mixed metal ion accumulation solutions (Cd (II), Pb (II), Cu (II) and Hg (II)) ($10^{-5}$ M for each cation) (**A**) and the dependence of the peak current in DPV ($\Delta i_{peak}$) on the q charge applied in CPE (**B**); **L**-CMEs were prepared at +1 V and different charges (0.5, 1, 6 mC).

The DPV curves shown in Fig. 5.11A for **L**-CMEs prepared by CPE at a potential of 0.5 V and a charge of about 2 mC show peaks for all metal cations in solution (Cu (II), Pb (II), Cd (II) and Hg (II)), at a concentration of $10^{-5}$ M (for each cation), but with different intensities. The highest analytical signals are recorded for Pb (II), followed by Hg (II). At lower concentrations of HMs ($10^{-6}$ M, $10^{-7}$ M and $10^{-8}$ M), **L**-CMEs show a better signal in DPV for Pb (II), showing a higher sensitivity for this cation compared to the other cations from the accumulation solutions. Figure 5.11B presents the calibration curve for the HMs analysis showing the dependence of the peak current in DPV for each metal ion *vs.* the concentration of the metal ion in the storage solutions. From the calibration curve it can be seen that the signal for Pb (II) increases linearly in the concentration range between $10^{-8}$ M - $10^{-7}$ M. At higher concentrations the signal reaches a limit value indicating a saturation starting from $10^{-6}$ M. At this concentration, the signal ratios for Pb (II)/ Hg (II)/ Cu (II)/ Cd (II) are of about in this order 19/ 8/ 4/ 1. These ratios highlight a high **L**-CMEs selectivity for Pb (II).

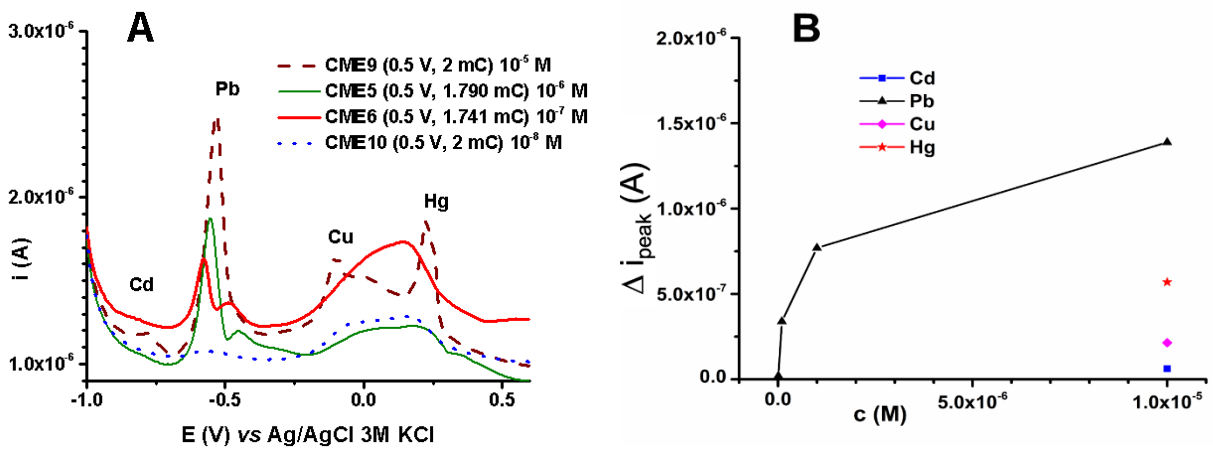


**Fig. 5.11.** Stripping DPV curves (0.01 V/ s) for **L**-CMEs after immersion in HMs mixed accumulation solutions of different concentrations ($10^{-5}$, $10^{-6}$, $10^{-7}$, $10^{-8}$ M) (**A**); dependence of peak currents in DPV

($\Delta i_{peak}$) on HMs concentrations for Pb, Cd, Cu and Hg (**B**); **L**-CMEs were prepared by CPE at +0.5 V and about 2 mC in a solution of **L** (1 mM) in 0.1 M TBAP/ $CH_3CN$.

## 5.2. CHARACTERIZATION OF **L**-CMEs SURFACE BY SCANNING ELECTRON MICROSCOPY (SEM) AND ATOMIC FORCE MICROSCOPY (AFM)

### 5.2.1. Materials and methods for SEM and AFM

The poly**L** films deposited on the pellet GC (d = 6 mm, OrigaLys Les Verchères, France) were prepared by CPE at different charges and potentials, according to Table 5.1, in 1 mM **L** solution and analyzed by SEM and AFM in order to determine the measure in which the conditions of film preparation influence their morphology.

Surface characterization of the new **L**-CMEs by SEM and AFM was performed according to a previously established procedure [5.2 - 5.5]. The surface roughness parameter (RMS) and average roughness (Ra) of the poly**L** films were calculated based on the topographic images generated by the processing software, as in the case of other azulene derivatives [5.6].

### 5.2.2. Surface studies for L-CMEs by SEM and AFM

The morphology of the poly**L** films deposited on the surface is given by the SEM and AFM images that allow to establish the characteristics of the polymer films (Table 5.7). The columnar structures observed in the SEM micrograph for **L**-CME prepared at +0.5 V and 28 mC/ $cm^2$ were also identified in the AFM measurements. These columnar structures have a maximum height of ~180 nm. The presence of these columns strongly influences the roughness of the sample.

The polymer surface becomes rougher and the RMS value increases from 3.38 nm to 4.81 nm when the charge density increases from 26 mC/ $cm^2$ to 28 mC/ $cm^2$. The film deposition time increases from 5000 s for 26 mC/ $cm^2$ to about 6000 s for 28 mC/ $cm^2$. From the results of the SEM column in Table 5.7 it can be concluded that at 28 mC/ $cm^2$ the formations are more prominent than at 26 mC/ $cm^2$, their sizes being similar: 9-14 nm for 28 mC/ $cm^2$ and 9-12 nm for 26 mC/ $cm^2$. From the AFM column of the same table, it follows that the maximum height of the columnar formations is approximately 180 nm at 28 mC/ $cm^2$, higher than for the film obtained at 26 mC/ $cm^2$ where areas with formation agglomerations with a maximum height of approximately 105 nm can be noted.

Both SEM and AFM experiments showed that the morphological properties and roughness of the poly**L** films are influenced by the electropolymerization parameters (charge, potential) applied in CPE.

**Table 5.7. SEM images obtained at 100 K magnification and 500 nm enlargement and AFM images (2D and 3D projections of topographic images) for bare GC and L-CMEs prepared by CPE at +0.5 V and approx. 8 mC in 1 mM L solution.**

| Sample | SEM image at 100 K | AFM image - 2D Projection | AFM image - 3D Projection |
|---|---|---|---|
| bare **GC** | 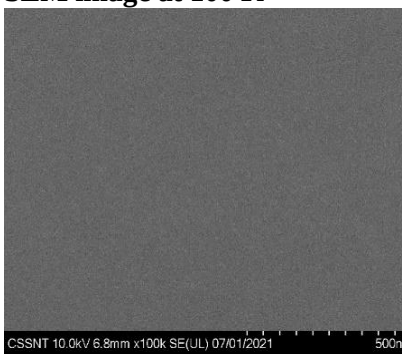  | 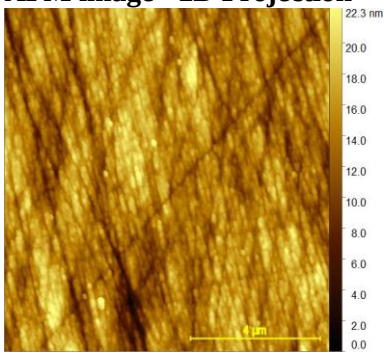  | 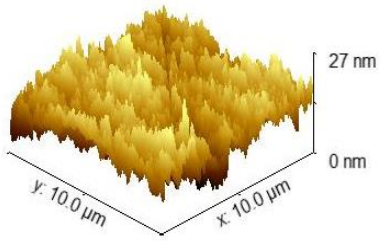  |
| **CMEp18** (+0,5 V; 26 mC/ $cm^2$) | 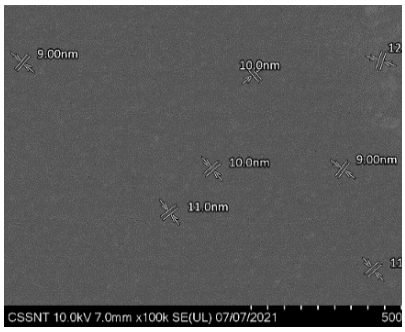  | 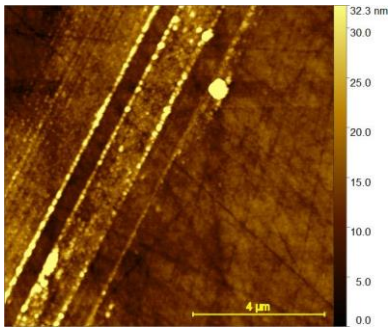  | 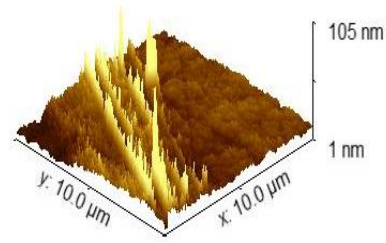  |
| **CMEp17** (+0,5 V; 28 mC/ $cm^2$) | 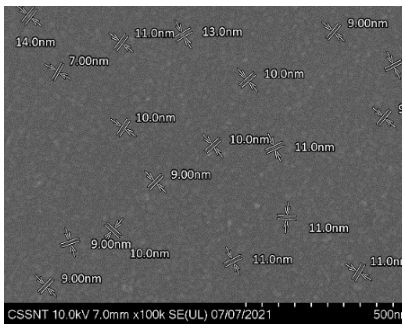  | 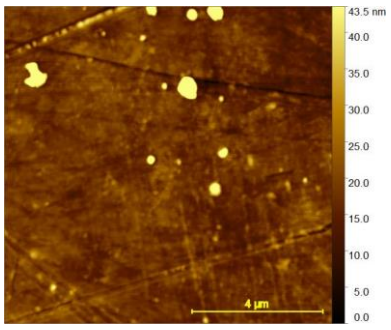  | 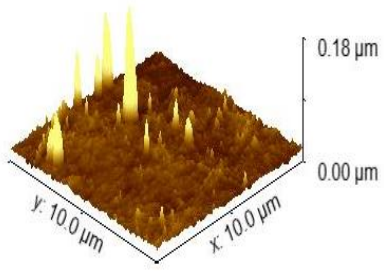  |

## 5.3. OPTIMAL PARAMETERS FOR THE PREPARATION OF **L**-CMEs

The study carried out in this chapter aimed to optimize the **L**-CMEs preparation stage by choosing the best electropolymerization conditions for the analysis of HMs ions. Several charge and potential values were tested to obtain **L**-CMEs by CPE in 1 mM **L** solutions in 0.1 M TBAP/ $CH_3CN$. For the films prepared at a potential of 0.5 V and the electropolymerization charge of about 2 mC (which corresponds to a charge density of 28 mC/ $cm^2$), the film deposition time was of several hours, and the ferrocene signal for **L**-CMEs in the transfer solution was highly disturbed compared to the bare GC electrode. Thus, the analytically optimal synthesis potential was determined to be +0.5 V (close to the a1 peak potential in the DPV curve, which is +0.55 V).

Therefore, the polymer films prepared at a potential of 0.5 V and a charge of about 2 mC were used to analyze cations ($Cd^{2+}$, $Pb^{2+}$, $Cu^{2+}$ and $Hg^{2+}$) in test solutions of different HMs concentrations. Good analytical signals were obtained for all investigated HMs ions in the mixed solution of $10^{-5}$ M concentration. At low concentrations (below $10^{-7}$ M), **L**-CMEs have a higher sensitivity for Pb (II) ions than for the other ions.

# CHAPTER 6
# CHARACTERIZATION OF THE SURFACE OF CHEMICALLY MODIFIED ELECTRODES WITH LIGAND 4-(AZULEN-1-YL)-2,6-BIS((E)-2-(THIOPHEN-2-YL)VINYL)PYRIDINE (M)

The characterization of the CMEs surface based on 4-(azulen-1-yl)-2,6-bis((E)-2-(thiophen-2-yl)vinyl)pyridine (denoted with **M**) was carried out using the following methods: scanning electron microscopy (SEM), energy dispersive X-ray spectroscopy (EDX), atomic force microscopy (AFM), Fourier transform IR spectroscopy (FTIR), and fluorescence (FL). The methods for characterizing the CMEs surface were chosen according to the desired uses of this monomer, namely the development of new electrochemical sensors for HMs detection, and for optical applications, respectively.

This chapter of the thesis presents the results obtained by SEM, AFM, FTIR and FL analyses of CMEs prepared in different ways using monomer **M**, whose chemical structure is shown in Fig. 6.1.

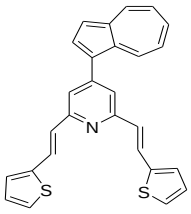


**Fig. 6.1.** Chemical structure of 4-(azulen-1-yl)-2,6-bis((E)-2-(thiophen-2-yl)vinyl)pyridine (**M**).

## 6.2. MATERIALS AND APPARATUS

**M** was synthesized according to the method described in literature [3.25, 6.3, 6.19, 6.25]. The preparation of CMEs followed a previously established procedure in the *EPOS* laboratory [6.16], namely by two methods: scanning (CV) and CPE.

For the SEM experiments, the QUANTA INSPECT F 50 scanning electron microscope equipped with a field emission gun - FEG, with a resolution of 1.2 nm, was used. EDX, elemental analysis on small areas, nanometer-size in diameter, was coupled to SEM.

The Park Systems XE-100 atomic force microscope was used to investigate surface topography. The RTESPA model AFM probe, doped with Si, was used for data acquisition. Image analysis was performed with SPM Lab Analysis v.7.0 special software (from Veeco Company). AFM (2D and 3D) images of organic films deposited on GC support were recorded. The surface of the samples was scanned in non-contact mode. The maximum horizontal scan range was 50×50 $\mu m^2$ and the maximum vertical movement was 8 μm. Depending on the scanning peaks, a lateral resolution of about 10 nm was obtained.

The Nanolog 3 - Horiba Jobin-Yvon spectrofluorimeter was used for the fluorescence experiments. The measurement conditions were as follows: excitation at 380 nm, emission filter at 399 nm, and wavelength range of 400 - 600 nm. The samples were excited at a wavelength of

380 nm to see their emission, using the filter positioned before the detector to cut the influence of the excitation.

### 6.3.1. Preparation of M-CMEs samples

**M**-CMEs were prepared from 1 mM solutions of **M** in 0.1 M TBAP/ $CH_3CN$ by successive scanning (the potential was varied from 0 V to different anodic potential limits +0.81 V, +0.91 V, +1.6 V) and by CPE at different potentials (+0.81 V, +0.91 V and +1.6 V) and charges (2 mC, 3.2 mC and 6 mC). Table 6.1 summarizes the conditions of film preparation, the type of investigation and their optical characteritics.

**Table 6.1. CMEs samples' preparation and testing conditions, and color of the obtained films.**

| Sample | Film formation | Type of investigation | Film color |
|---|---|---|---|
| **1** | Scanning +0,81 V, 15 cycles | SEM, EDX, FTIR, FL | Blue |
| **2** | Scanning +0,91 V, 15 cycles | SEM, EDX, FTIR, FL | Turquoise |
| **3** | Scanning +1,6 V, 10 cycles | SEM, EDX, FTIR, FL | Brown |
| **4** | CPE +0,81 V, 6 mC | AFM | Emerald green |
| **5** | CPE +0,91 V, 6 mC | SEM, EDX, AFM, FTIR, FL | Blue |
| **6** | CPE +1,6 V, 6 mC | AFM | Gray |
| **7** | CPE +0,91 V, 2 mC | - | Dark turquoise |
| **8** | CPE +0,91 V, 3,2 mC | SEM, EDX, FTIR, FL | Greenish yellow |
| **9** | CPE +0,81 V, 2 mC | AFM | Navy blue |
| **10** | CPE +0,81 V, 3,2 mC | AFM | Yellow-green |

### 6.3.2. Results and discussions on the characterization of the M-CMEs surface by SEM and EDX methods

Films prepared by CPE show uniform surfaces with rare nanoclusters. Thicker films obtained using a charge of 6 mC show larger nanocluster sizes (150 - 250 nm) than those obtained with a charge of 3.2 mC (100 - 200 nm), the electropolymerization potential being the same 0.91 V (Fig. 6.2). However, thinner films prepared by CPE using a charge of 3.2 mC have more nanoclusters per unit area compared to those prepared at 6 mC. For samples 1 - 3 prepared by scanning, increasing the potential leads to the formation of nanostructured or rough polymer films. The film obtained by scanning at 0.91 V showed a nanostructured surface with dimensions of 3 - 11 nm, and for the film obtained by the same method at 1.6 V it was found to also present a nanostructured surface with dimensions of 8.5 - 22 nm, as shown in Fig. 6.3.

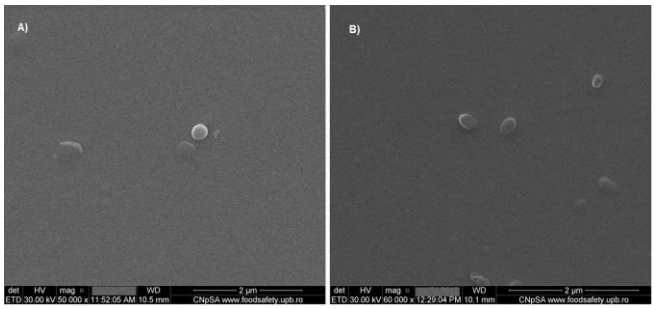


**Fig. 6.2.** SEM images of CMEs obtained by CPE at +0.91 V and different electropolymerization charges: (**A**) 6 mC for sample 5; (**B**) 3.2 mC for sample 8.

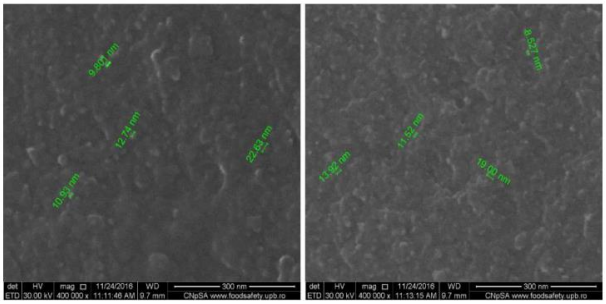

**(a)** **(b)**

**Fig. 6.3.** SEM images for sample 3 with nanometer structures of 9.8 nm - 22.6 nm (**a**) and 8.5 nm - 19 nm (**b**).

### 6.3.3. Results and discussions on the characterization of the M-CMEs surface by the AFM method

Figure 6.6 shows the 2D and 3D images for sample 5 obtained at a large scale (nm/ div = 200) which highlight the scattered grains. Sample 5 shows a very rough surface, with a roughness value of 35.8 nm due to the presence of large grains with sizes around 1 μm. These dispersed granules appear to be formed by the aggregation of NPs with sizes between 200 - 500 nm.

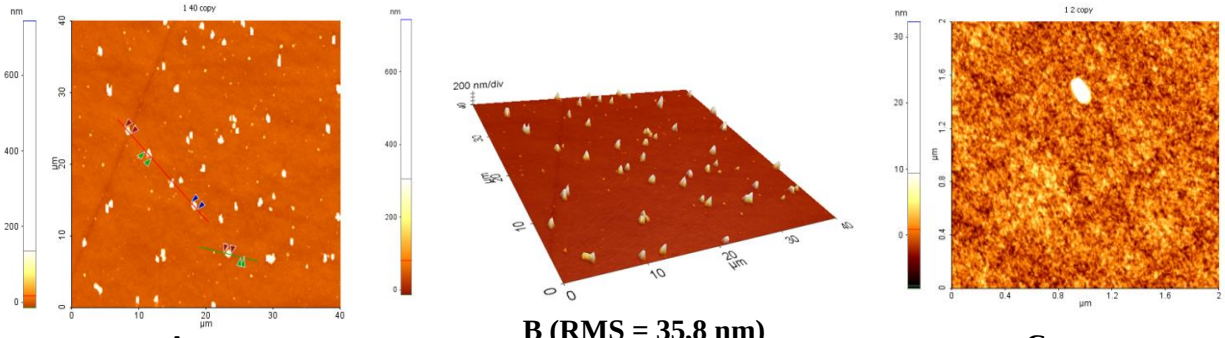


**A** **B (RMS = 35,8 nm)** **C**

**Fig. 6.6.** AFM images for sample 5 prepared by CPE (+0.91 V, 6 mC): (**A**) 2D image for the 40x40 μm$^2$ surface; (**B**) 3D image for the 40x40 μm$^2$ surface; (**C**) 2D image for the 2x2 μm$^2$ surface.

The AFM topography showed the presence of column-shaped features with a maximum height of 150 nm on the surfaces of **M**-CMEs. The RMS values calculated based on the topographic images and presented in Table 6.3 show the influence of the charge and the electropolymerization potential on the surface roughness for the studied CMEs. The RMS results for **M**-CMEs prepared by CPE at the same potential of 0.81 V, but using different charges (2, 3.2 and 6 mC), are in the same range of values, so the influence of the electropolymerization charge on the roughness is not significant at this potential. Images of polymer layers prepared by CPE at a constant charge of 6 mC, but at variable potentials (0.81, 0.91 and 1.6 V) indicate that, at the intermediate potential of 0.91 V, surfaces with the highest roughness are obtained. This value corresponds to the electropolymerization potential for which the better analytical signal was reported for **M**-CMEs prepared under the same conditions and used in the analysis of HMs ions in synthetic water samples. In this way, surface roughness can be correlated with the analytical performance of polymer layers deposited by CPE on GC [3.25, 6.19]. This can be explained by

the increase of the active surface due to the presence of large granules with dimensions around 1 μm, which are supposed to have been formed by the aggregation of NPs with dimensions between 200 - 500 nm.

**Table 6.3. RMS results obtained from AFM data for the investigated samples.**

| Sample | Film formation parameters | RMS for 40x40 μm$^2$ surfaces | RMS for 2x2 μm$^2$ surfaces |
|---|---|---|---|
| **9** | CPE 0,81 V, 2 mC | 2,4 | 2,0 |
| **10** | CPE 0,81 V, 3,2 mC | 5,2 | 2,0 |
| **4** | CPE 0,81 V, 6 mC | 4,2 | 2,4 |
| **5** | CPE 0,91 V, 6 mC | **35,8** | 2,2 |
| **6** | CPE 1,6 V, 6 mC | 2,9 | 2,5 |

### 6.3.4. Results and discussions on the characterization of the M-CMEs surface by the FTIR method

The FTIR spectra shown in Fig. 6.8 were recorded for CMEs prepared by scanning (samples 1 - 3) and by CPE (samples 5 and 8) according to Table 6.1. Minimum values of transmittance (T) were detected only for samples prepared by CPE at a constant potential of +0.91 V and 3.2 mC (sample 8) and 6 mC (sample 5), respectively, and are attributed to the presence of thiophene and the thiophene's specific bonding to pyridine. It can be said that the complexation units in these films remain intact following the electropolymerization process.

Fluorescence spectra were recorded for the samples obtained by scanning (samples 1 - 3) shown in Fig. 6.10A and by CPE (samples 5 and 8) of Fig. 6.10B. The fluorescence spectra in the mentioned figures show that the samples prepared by scanning (samples 1 - 3) have higher fluorescence intensity than those prepared by CPE (samples 5 and 8). As the anodic limit of the scanned potential increases, the fluorescence decreases. The fluorescence of thicker poly**M** films prepared by CPE is higher. All investigated samples (1 - 3, 5 and 8) present a broad emission band extended between 400-600 nm, with different peak positions. These results show that the polymerization by scanning preserves the fluorescence properties of poly**M** films, while polymerization by CPE limits the fluorescence of the polymer film. This conclusion is important for future optical applications of these polymer films.

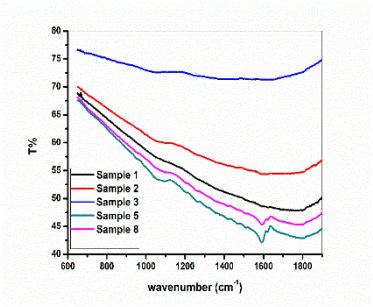


**Fig. 6.8.** FTIR spectra for samples prepared by scanning (samples 1 - 3) and CPE (samples 5 and 8).

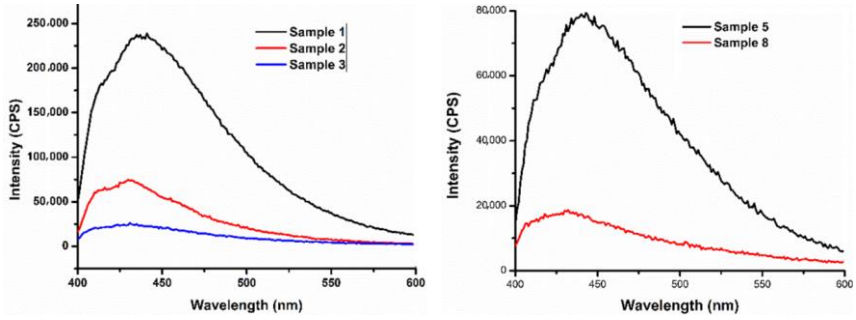


**A** **B**

**Fig. 6.10.** Fluorescence spectra for samples prepared by scanning (samples 1 - 3) (**A**) and CPE (samples 5 and 8) (**B**).

### 6.3.6. Highlighting the formation of films by electrochemical methods

The electrochemical studies of monomer **M** containing complexing fragments of pyridine symmetrically substituted with (thiophen-2-yl)vinyl were performed by CV, DPV and RDE, as in Fig. 6.12, to confirm the formation of polymer films, differently colored, as mentioned in Table 6.1.

The increase of the peak current in the a3 peak domain with the increase of the monomer **M** concentration is more obvious for the CV and DPV curves than for the RDE curves, a fact correlated with the formation of insulating films at potentials more positive than the a3 peak, which is confirmed by the cyclic voltammograms in Fig. 6.13B.

More evidence of polymer film formation on GC was obtained during the preparation of **M**-CMEs by scanning. Figure 6.13A shows successive CV curves up to +0.8 V where cycle 1 is different from the following ones, which were shifted to more positive potentials. After a decrease between cycle 1 and cycle 2, the peak currents increase by cycling the potential as the number of cycles advances. For peak a1, several characteristics specific to the formation of films were observed: irreversibility of the peak, movement of the peak potential in cycle 2 towards more positive values than in cycle 1, appearance of a new redox couple around the potential of +0.3 V specific to the reversible process of oxidation and reduction of the polymer and increasing peak currents for this couple with the number of cycles. In Figures 6.12 and 6.13A, it can be seen that polymerization occurs at the a1 peak potential, but proceeds in a different way than at the a3 peak potential, leading to a conductive film.

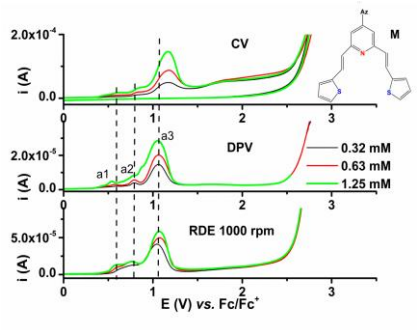


**Fig. 6.12.** CV, DPV and RDE curves for **M** (Az stands for azulen-1-yl) at different concentrations (mM) in 0.1 M TBAP/ $CH_3CN$ at scan in the anodic range.

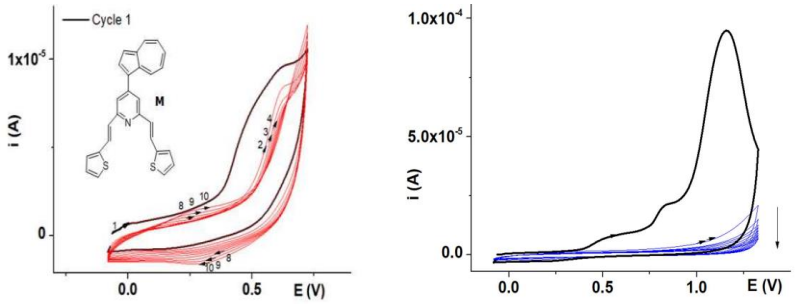


**Fig. 6.13.** CV curves (0.1 V/ s) during the preparation of CMEs by scanning the potential in the domain of the anodic peak a1 (**A**) and over a wider potential domain (over peak a3) (**B**) for **M** (0.63 mM) in 0.1 M TBAP/ $CH_3CN$.

The CV curves for 1 mM **M** solution in 0.1 M TBAP/ $CH_3CN$ obtained at different scan rates show that peak current values increase with the scan rate (Figures 6.14A and 6.14B). Linear dependences of the peak currents on the square root of the scan rate were obtained, with different slopes for a1 - a3 that increase significantly from peak a1 to peak a3, as shown in Fig. 6.14C. This fact can be explained by assuming that different films are formed if the electropolymerization is carried out at potentials in the domain of the a1 and a3 peaks.

The use of the CV, DPV and RDE voltammetric methods, which highlight the deposition of the polymer on the GC, allowed to establish that the potential values favorable to the formation of the films are between 0.8 V and 1 V.

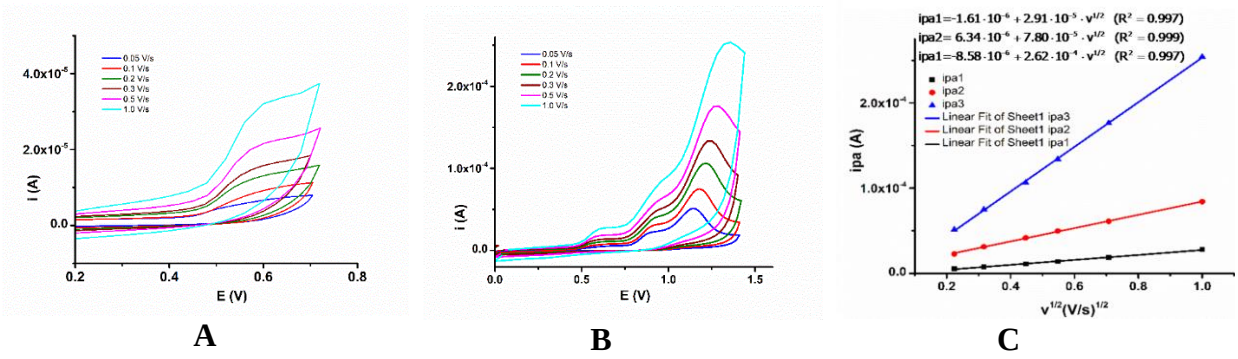


**Fig. 6.14.** CV curves for **M** (1 mM) in 0.1 M TBAP/ $CH_3CN$ obtained at different scan rates (0.05 - 1 V/ s), when scanning in the potential domains of peaks a1 (**A**) and a1 - a3 (**B**) and the linear dependence of the peak current (ipa) for peaks a1, a2 and a3 on the square root of the scan rate ($v^{1/2}$) (**C**).

Four GC electrodes (d = 3 mm) modified with poly**M** films were used to evaluate the reproducibility when analyzing different concentrations of Pb (II) ions in mixed accumulation solutions. The best analytical signals were recorded for Pb (II) and Hg (II) ions in mixed solutions of $10^{-6}$ M and $10^{-5}$ M concentrations. The peak currents for Pb (II) are higher than the currents of peak for Hg (II), showing that **M**-CMEs complex the Pb (II) ion selectively. The estimated error of the stripping DPV curves was below 5%.

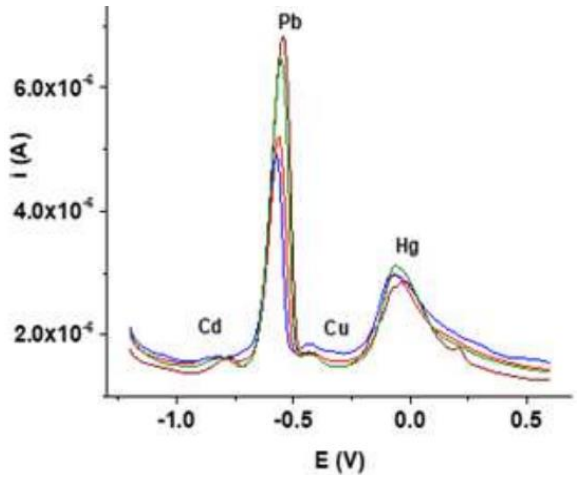


**Fig. 6.18.** DPV curves (0.01 V/ s) for CMEs prepared by CPE at +1.2 V and 0.5 mC in solution of **M** (0.63 mM) in 0.1 M TBAP/ $CH_3CN$ and introduced into mixed solutions of different concentrations: $10^{-6}$ M (blue and red) and $10^{-5}$ M (olive and wine).

# CHAPTER 7
# THE PROCESSING OF EXPERIMENTAL DATA OBTAINED ON SOIL AND PLANT SAMPLES BY STATISTICAL METHODS

## 7.1. METHODS OF STATISTICAL ANALYSIS APPLIED IN THE PERFORMED STUDIES

The processing and statistical interpretation of the experimental results obtained on soil and plant samples taken from the area of the aluminum plant in Slatina between 2011 - 2012 and 2019 was carried out using the exploratory analysis correlated with the formal statistical analysis. Parametric Two - Sample T-Test and non-parametric Kruskal - Wallis H and Dunnett's statistical tests were applied to determine the level of soil pollution with heavy metals and the influence of pollution on plants.

### 7.2.2. Kruskal-Wallis H and Dunnett tests applied to the experimental results obtained on soil and plant samples

The exploratory analysis of the experimental results obtained on soil and plant samples followed the distribution of elements with toxic potential in the soil sampled in the period 2011-2012 from the vicinity of the polluting source, namely from the rhizosphere of the plantain plant (10 plant replicates) and from two areas coded with C1 and C2 (6 replicates from each area), and in the soil sampled in 2019, from the same C1 and C2 areas, marked with C1.1 and C2.1 (5 replicates from each area). The analyzed soil groups were marked with: group 1 - reference soil 2011, group 2 - plantain rhizosphere soil 2012, group 3 - soil 2011 and group 4 - soil 2019. The statistical significance of the differences between the median values (calculated according to the relationships presented in references [7.1] and [7.2]) of the 4 analyzed groups is presented in Table 7.2, and the distribution of element concentrations presented comparatively is given in Figures 7.7 and 7.9. The reference soil in group 1 is a fertile soil, having a texture similar to the analyzed soil, namely yellow-brown clay soil with calcareous concretions [7.11].

Exploratory analysis and the Kruskal - Wallis H test were performed in Matlab version 2021a, and the RStudio software version 1.4.1106 was used for the Dunnett's test.

The Kruskal - Wallis H test [7.5] denied the equality of the medians, and the test results presented in Table 7.2 showed that, in the case of the 4 analyzed metals (Cu, Ni, Pb, Zn), there are statistically significant differences between the 4 groups, since the p value < 0.05.

**Table 7.2. The statistical significance of the differences between the values of the medians calculated on the basis of the Kruskal - Wallis H test.**

| **Elements** | **Group 1** | **Group 2** | **Group 3** | **Group 4** | **Kruskal - Wallis H-Test** |
|---|---|---|---|---|---|
| | R (2011) (n=8) | Plantain (2012) (n=10) | C1+C2 (2011) (n=12) | C1.1+C2.1 (2019) (n=10) | p value for 1-2-3-4 |
| **Cu** | | | | | |
| (μg/g) | 33,84 | 25,26 | 17,72 | 21,49 | $2{,}8 \cdot 10^{-6}$ |
| Average/DS | 1,54 | 5,18 | 4,31 | 1,83 | |
| Median | 33,71 | 23,80 | 16,51 | 21,47 | |

| | | | | | |
|---|---|---|---|---|---|
| **Ni** | | | | | |
| (µg/g) | 52,67 | 98,71 | 62,28 | 32,49 | $2 \cdot 10^{-6}$ |
| Average/DS | 3,96 | 16,93 | 36,70 | 4,53 | |
| Median | 52,25 | 95,26 | 58,24 | 34,65 | |
| **Pb** | | | | | |
| (µg/g) | 28,72 | 11,84 | 22,82 | 14,27 | $3,2 \cdot 10^{-7}$ |
| Average/DS | 2,85 | 2,46 | 2,26 | 1,86 | |
| Median | 27,89 | 11,28 | 23,01 | 13,75 | |
| **Zn** | | | | | |
| (µg/g) | 127,06 | 73,24 | 75,07 | 47,80 | $5,8 \cdot 10^{-7}$ |
| Average/DS | 8,27 | 8,23 | 5,42 | 6,79 | |
| Median | 124,45 | 71,03 | 76,53 | 45,37 | |

In Fig. 7.7 (left-hand image), it is observed that the dispersion of Cu concentration values in group 2 is greater than in groups 1, 3 and 4 (longer segments starting from the median up and down). In group 3, the range of concentration values (ranging between the maximum and minimum values) is higher than in group 4, and the median value (red line) is lower in group 3 compared to group 4. Compared to group 1 (soil reference), the Cu concentrations in groups 2, 3 and 4 show lower values, the lowest values being in group 3 where a Cu deficiency is recorded (17.72 µg/ g) and in group 4 which is poor in Cu (21.49 µg/ g). These average values are below the legal limit allowed in soil for plant growth (30 - 100 µg/ g). Outliers marked with "+" in groups 3 and 4 can be explained on the basis of soil heterogeneity.

In Fig. 7.7 (right-hand image), it can be seen that the range of values and the median value in group 2 are higher than in groups 1, 3 and 4. Between groups 2 and 4 there is no overlap of Ni concentration distributions, which is also confirmed by the value of p ($p<0.05$) indicating statistically significant differences between the two groups. Outliers are found only in group 3 and can be explained on the basis of the heterogeneity of the soil polluted with the toxic element Ni.

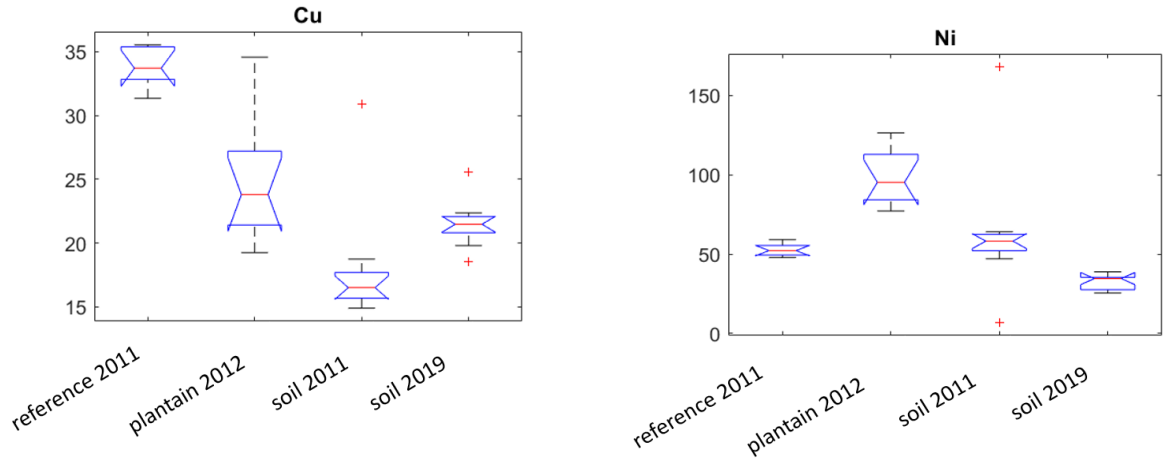


**Fig. 7.7.** Distribution of Cu (left) and Ni (right) concentration values in the soils of the polluted area compared to the reference area.

In Fig. 7.9 (left-hand image), it is observed that the dispersion of Pb concentration values in group 2 is greater than in groups 1, 3 and 4. Between groups 1, 3 and 4 there is no overlap of Pb concentration distributions, which confirms that between groups taken two by two there are statistically significant differences ($p<0.05$). Between groups 3 and 4, the dispersion of the Pb

concentration values and the median value are smaller in group 4, with the mention that, in group 4, the median value is in the vicinity of the minimum value of the Pb concentration, indicating the asymmetry of the distribution (non-Gaussian). Outliers are found in groups 1, 3 and 4.

The distribution of Zn concentration values in the analyzed soils shown in Fig. 7.9 (right-hand image) shows that the range of values in group 2 is larger than in groups 1, 3 and 4. The dispersion of Zn concentration values and the median value in group 4 are smaller than in groups 1, 2 and 3, which shows that the soil is relatively poor in Zn. Outliers are found only in group 4.

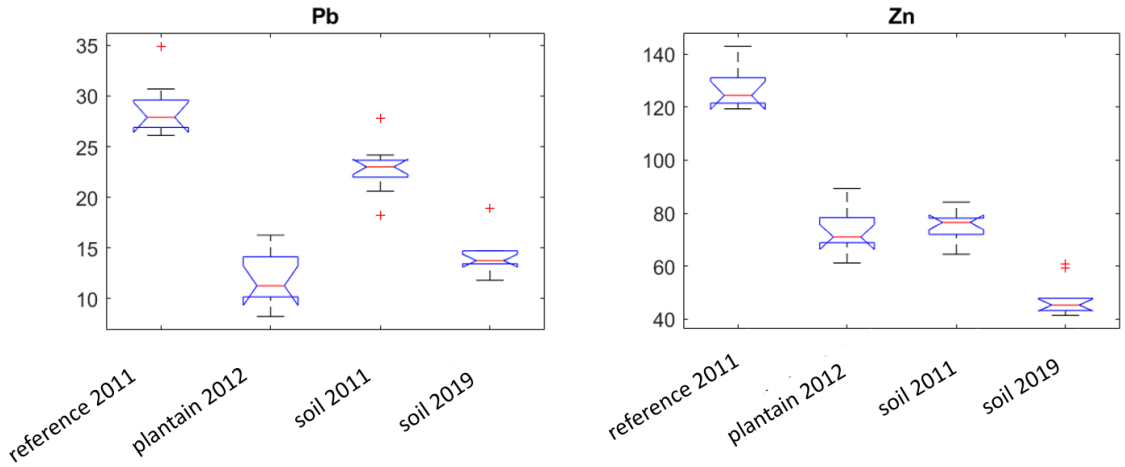


**Fig. 7.9.** Distribution of Pb (left) and Zn (right) concentration values in the soils of the polluted area compared to the reference area.

The exploratory analysis and the Kruskal - Wallis H test applied to evaluate the differences between the median concentrations of Cu, Ni, Pb and Zn elements in the 4 analyzed soils (reference soil 2011, plantain rhizosphere soil 2012, soil 2011 and soil 2019) showed that the values compared are different ($p<0.05$), the distribution of Zn and Ni concentrations in soil 2019 recording the lowest values. The research carried out showed a decrease in soil pollution with toxic elements in 2019 compared to the period 2011 - 2012, which could lead to a decrease in the plant oxidative stress.

# CONCLUSIONS

## C1. GENERAL CONCLUSIONS

Within the framework of this PhD thesis entitled "**CHEMICALLY MODIFIED ELECTRODES WITH APPLICATIONS IN THE CONTROL OF SOIL AND PLANT POLLUTION WITH INORGANIC POLLUTANTS IN THE SLATINA INDUSTRIAL AREA**", the research areas approached aimed at identifying and developing the most appropriate methods capable of detecting and reducing the content of inorganic pollutants (especially heavy metals) in contaminated environments, thus preventing their entry into the food chain. The development of electrochemical sensors capable of detecting low heavy metal concentrations in the environment represents an alternative to other more expensive analytical methods, such as inductively coupled plasma mass spectrometry (ICP-MS) and flame atomic absorption spectrometry (F-AAS) applied to the polluted soil in the area of the aluminum plant in Slatina.

The development of new electrochemical devices capable of monitoring inorganic pollutants, such as heavy metals, addressed in the PhD thesis, is a concern of the research group of the Electrochemical Processes in Organic Solvents (*EPOS*) laboratory in the Department of Inorganic Chemistry, Physical Chemistry and Electrochemistry within the Faculty of Chemical Engineering and Biotechnologies affiliated to the POLITEHNICA University in Bucharest, of which I belong and where the PhD thesis was developed.

The studies carried out and presented in PART II - **ORIGINAL CONTRIBUTIONS** of this paper led to the following general conclusions:

**Chapter 4** of the PhD thesis presents the results of the studies carried out to obtain new chemically modified electrodes (CMEs) based on the azulene-tetrazole derivative E-5-((5-isopropyl-3,8-dimethylazulen-1-yl)diazenyl)-1H-tetrazole (**L**) which exhibits complexing and recognition properties of heavy metal ions. The new azulene-tetrazolic derivative (**L**) was synthesized by the researchers of the *C. D. Nenițescu* Center of Organic Chemistry of the Romanian Academy. The electrochemical characterization of ligand **L** by voltammetric methods (CV, DPV and RDE) showed the formation of two peaks in the anodic range (a1, a2) and five peaks in the cathodic range of potentials (c1, c2, c3, c4 and c5). **L**-based chemically modified electrodes (**L**-CMEs) were prepared by successive cycling (20 cycles) in the anodic range at different potentials (0.75 V, 1 V) or by controlled potential electrolysis (CPE) using different charges and potentials (1 mC and 0.75 V, 1 mC and 1 V, 2 mC and 1 V). The complexation properties of **L**-CMEs prepared by CPE in 1 mM **L** solution in 0.1 M TBAP/ $CH_3CN$ at 1 V potential and 1 mC charge were studied to evaluate the ability of polymer films to complex heavy metal ions. By chemical preconcentration and anodic stripping using **L**-CMEs, metal cations (Cu (II), Pb (II), Cd (II) and Hg (II)) were detected from synthetic aqueous solutions having concentrations between $10^{-8}$ M and $10^{-4}$ M. Well-defined recognition peaks were obtained for Pb (II) and Hg (II) in mixed solutions having concentrations of $10^{-5}$ M and $10^{-4}$ M, respectively, showing that **L**-CMEs prepared at 1 V and 1 mC show high selectivity towards Pb (II) and Hg (II). A good analytical signal was obtained for the Pb (II) ion in the mixed solution of $10^{-8}$ M concentration. The obtained results show that the **L**-CMEs prepared at 1 V and 1 mC show a selective complexation for Pb (II), with possibilities of analyzing these cations in water samples at a detection limit estimated at $10^{-8}$ M. The ability of ligand **L** to form complexes with Pb (II) and Hg (II) ions was evaluated by UV-Vis spectrophotometric techniques. By spectrophotometric titration of **L** 7.06 μM in $CH_3CN$ with increasing concentrations of Pb (II) ions, respectively Hg (II) in a molar ratio of 0.2; 0.4; 0.6; 0.8; 1.0; 1.2; 1.4; 1.6; 1.8; 2.0; 2.5 and 3.0 to 1, hypo, batho, hyper, and hypso-chromic shifts of the five absorption bands of ligand **L** were recorded. The formation of isosbestic points in the UV-Vis spectra confirmed the existence in solution of uncomplexed monomer **L** and of the coordinated complexes formed between Me and **L**. The same stoichiometry of Me(II):**L** = 1:2 complexes was determined by applying the molar ratio method and the continuous variations method (Job's method). Ligand **L**'s complexation properties studied by UV-Vis spectroscopy and of **L**-CMEs investigated by the DPV method revealed a high selectivity for the Pb (II) ion.

**Chapter 5** of the thesis presents the results of the research carried out to improve the conditions for the **L**-CMEs preparation (potential, charge) presented in Chapter 4 in order to analyze HMs ions at low concentrations in different water samples. In order to choose the optimal parameters of the electropolymerization process for **L**-CMEs prepared by CPE in 1 mM **L** solution in 0.1 M TBAP/ $CH_3CN$ on standard GC (d = 3 mm) and pellet GC (d = 6 mm) electrodes, several potential and charge values were tested. **L**-CMEs were characterized by cyclic voltammetry during transfer in 0.1 M TBAP/ $CH_3CN$ supporting electrolyte or in 1 mM ferrocene solution in 0.1 M

TBAP/ $CH_3CN$. The complexation properties of the **L**-CMEs that showed the most flattened ferrocene signal as compared to the bare GC electrode were investigated. The optimal electropolymerization parameters of 0.5 V and 2 mC were established, and the polymer films prepared under these conditions were used for the recognition of HMs ions (Cu (II), Pb (II), Cd (II) and Hg (II)) in synthetic aqueous solutions having concentrations between $10^{-8}$ M and $10^{-5}$ M. The DPV curves showed well-defined peaks for all investigated ions in the mixed solution of $10^{-5}$ M concentration, but the analytical signals vary in this order: Pb>Hg>Cu>Cd. At lower concentrations of HMs ($10^{-6}$ M, $10^{-7}$ M, $10^{-8}$ M), **L**-CMEs showed a higher selectivity for Pb (II), the detection limit being about $10^{-8}$ M. The surface morphology of the **L**-CMEs prepared by CPE at different potentials and charge densities on pellet GC (d = 6 mm) investigated by SEM and AFM revealed that the surface-deposited poly**L** films exhibit columnar formations that are more prominent at the potential of 0.5 V and the charge density of 28 mC/ $cm^2$ (it corresponds to a charge of 2 mC). The results obtained by SEM and AFM measurements are confirmed by the surface roughness parameter (RMS) which has higher values when the film is thicker. By micro-Raman spectroscopy it was established that poly**L** films obtained at a potential of 0.5 V and a charge density of about 28 mC/ $cm^2$ behave in a similar way to the multilayered graphene network.

**Chapter 6** of the thesis presents the results of the research carried out for the surface characterization of the new CMEs based on the monomer 4-(azulen-1-yl)-2,6-bis((E)-2-(thiophen-2-yl)vinyl)pyridine (**M**) in order to detect heavy metal cations. The surface morphology of **M**-based CMEs (**M**-CMEs) prepared by scanning (CV) and CPE in 1 mM solutions of **M** in 0.1 M TBAP/ $CH_3CN$ was investigated by SEM, AFM, FTIR and fluorescence analyses. The information obtained by SEM and EDX analyses for the investigated samples were correlated with the RMS values determined by the AFM technique and with the results obtained by fluorescence studies. The surface-deposited poly**M** films analyzed by SEM coupled with EDX show different properties depending on electropolymerization conditions (potential, charge). The AFM analysis of **M**-CMEs prepared by CPE at different charges and potentials showed the presence of columnar formations with a maximum height of 150 nm. The RMS results revealed that the polymer film prepared by CPE at the potential of 0.91 V and the charge of 6 mC shows the roughest surface (35.8 nm) corresponding to a higher charge of electropolymerization. At the same potential value of 0.91 V, a better analytical signal was recorded for the **M**-CMEs used in HMs ion detection. The minimum values of transmittance (T) for **M**-CMEs prepared by CPE collected from FTIR spectra are attributed to thiophene and pyridine bondings. It can be assumed that the azulene electropolymerization is of the π-type (π-stacking). Through fluorescence studies of the **M**-CMEs surface, it was established that the polymerization by scanning preserves the fluorescence properties of poly**M** films, while that the polymerization by CPE limits the fluorescence of the polymer film. These methods (SEM, AFM, FTIR and fluorescence) used to characterize the surfaces of **M**-based CMEs revealed certain properties of the polymer films that can be exploited depending on the fields of use of monomer **M**.

**Chapter 7** of the thesis presents the statistical interpretation of the experimental results obtained on soil and plant samples sampled from the area of the aluminum plant in Slatina during 2011 - 2012 and 2019 by applying parametric and non-parametric statistical tests. The exploratory analysis of each data set was carried out with the help of boxplot diagrams in which the values of the distribution were represented: "minimum value, first quartile, median, third quartile and maximum value" [7.1]. The formal statistical analysis was performed by applying the parametric Two - Sample T-Test and the non-parametric Kruskal - Wallis H-Test and Dunnett's Test. The Two - Sample T test applied to the physico-chemical parameters of the soil in areas with different pollution (the aluminum plant area and the area of transects A and B) showed the existence of

statistically significant differences between the soils, with a few exceptions. The difference between the average values of As, Cr and Mn concentrations in the two areas with different pollution shows that in the vicinity of the plant the pollution was polymetallic and caused the occurrence of oxidative stress in plants. The Kruskal - Wallis H test applied to evaluate the differences between the median concentrations of Cu, Ni, Pb and Zn elements in the four soils analyzed (reference soil 2011, plantain rhizosphere soil 2012, soil 2011 and soil 2019) showed statistically significant differences ($p < 0.05$) between all analyzed soils. By applying the Dunnett test to the four analyzed soils, grouped two by two, statistically significant differences ($p<0.05$) were recorded, with a few exceptions, which were confirmed by calculating the 95% confidence interval for each metal. The statistical studies carried out showed a decrease in toxic elements soil pollution in 2019 compared to the period 2011 - 2012, which could lead to a decrease in the oxidative stress of the plants due to the presence of heavy metals.

## C2. ORIGINAL CONTRIBUTIONS

The original contributions presented by the PhD thesis are:

- Electrochemical study of a new azulene-tetrazole derivative E-5-((5-isopropyl-3,8-dimethylazulen-1-yl)diazenyl)-1H-tetrazole (**L**) by CV, DPV and RDE, and obtaining new **L**-based CMEs;
- Characterization of newly obtained **L**-CMEs by electrochemical techniques (CV) and surface analysis (SEM, AFM, micro-Raman spectroscopy);
- Investigating the complexation properties of ligand **L** by UV-Vis spectroscopy;
- Detection of HMs (Cu (II), Pb (II), Cd (II) and Hg (II)) in aqueous solutions of different concentrations using **L**-CMEs;
- Optimization of electropolymerization parameters (potential, charge) to obtain new **L**-CMEs in order to improve HMs detection limit;
- Characterization of the surfaces of the new CMEs based on the monomer 4-(azulen-1-yl)-2,6-bis((E)-2-(thiophen-2-yl)vinyl)pyridine (**M**) by structural analysis techniques (SEM), EDX, AFM, FTIR and fluorescence) in order to detect HMs ions;
- Application of parametric and non-parametric statistical tests to follow the evolution over time of heavy metal concentrations in the analyzed soils and their influence on plants.

## C3. PROSPECTS FOR FURTHER DEVELOPMENT

The research carried out in this PhD thesis provides new insights related to:

- The electrochemical study of new complexing azulenic derivatives with the aim of developing a broad base of azulenic compounds as monomers to obtain CMEs;
- Establishing the optimal parameters to obtain the new CMEs with applications in the detection of HMs at low concentrations in different water samples;
- Improving the performance of the new CMEs in order to obtain electrochemical sensors that allow the detection and field monitoring of HMs in polluted areas;
- Detailed studies to reduce the oxidative stress of plants grown on HMs polluted lands.

# ANNEXES

## A.1. ARTICLES PUBLISHED DURING THE DOCTORAL THESIS

1. *I.-G. Bugean, **A. Păun**, E. Diacu, M. Cristea, L. Bîrzan and E.-M. Ungureanu*, "Chemically modified electrodes based on 4-(azulen-1-yl)-2,6-bis((E)-2-(thiophen-2-yl)vinyl)pyrylium perchlorate", in Revista de Chimie, **vol. 71**, no. 9, 2020, pp. 113-124, indexed BDI. IF = 0.
2. *E. Diacu, **A. Păun**, V. Anăstăsoaie, G.-L. Arnold-Tatu, L. Bîrzan and E.-M. Ungureanu*, "Electroactive properties of a new azulene thioxo-imidazolidin-4-one ligand for modified electrodes", in Journal of Electrochemical Science and Engineering, **vol. 10**, no. 2, March, 2020, pp. 209-217, indexed Q3. IF = 0.
3. ***A.-M. Păun**, O.-T. Matica, V. Anăstăsoaie, L.-B. Enache, E. Diacu and E.-M. Ungureanu*, "Recognition of heavy metal ions by using E-5-((5-isopropyl-3,8-dimethylazulen-1-yl) dyazenyl)-1H-tetrazole modified electrodes", in Symmetry, **vol. 13**, no. 4, April, 2021, 644 - **PRECISI Award**. IF = 2.645, IRS = 0.687, IAS = 0.435.
4. ***A.-M. Păun**, O.-T. Matica, L.-B. Enache, E. Diacu, E.-M. Ungureanu and M. Enăchescu*, "Studies to improve the performance of chemically modified electrodes based on E-5-((5-isopropyl-3,8-dimethylazulen-1-yl)diazenyl)-1H-tetrazole for heavy metal ions analysis", in U.P.B. Sci. Bull., Series B, **vol. 84**, no. 4, 2022, pp. 3-20. IF = 0.
5. *I. Chilibon, **A.-M. Păun**, C. Vasiliu, E. Diacu, R. Isopescu and E.-M. Ungureanu*, "Surface characterization of modified electrodes based on 4-(azulen-1-yl)-2,6-bis((E)-2-(thiophen-2-yl)vinyl)pyridine", in Symmetry, **vol. 14**, no. 12, Nov. 2022, 2506. IF = 2.940, IRS = 0.1145, IAS = 0.435.

Cumulated IF (position 3+5) = 5.585; cumulated IRS (position 3+5) = 0.8015; cumulated IAS (position 3+5) = 0.870.

## A.2. SCIENTIFIC PAPER SESSIONS DURING THE DOCTORAL THESIS

1. Alexandru Anton Ivanov, Elena Diacu, Eleonora-Mihaela Ungureanu, Sabina-Vasilica Pistol, **Adinuța Păun**, Magdalena-Rodica Bujduveanu, *Analytical applications of new chemically modified electrodes based on crown eter for heavy metal analysis*, 7th Regional Symposium on Electrochemistry for South-East Europe (RSE-SEE-7), 27$^{th}$-30$^{th}$ May, 2019, Split, Croatia, EAS-P-5.
2. **Adinuța Păun**, Elena Diacu, *The response of some plants to the oxidative stress caused by heavy metal soil pollution in the industrial area of Slatina*, 21st Romanian International Conference on Chemistry and Chemical Engineering, 4$^{th}$-7$^{th}$ September, 2019, Constanța-Mamaia, Romania, Poster (S5-188).
3. **Adinuța Păun**, Elena Diacu, Alina-Giorgiana Brotea, Eleonora-Mihaela Ungureanu, *Recognition of heavy metal ions by using electrodes modified with E-5-((5-isopropyl-3,8-dimethylazulen-1-yl)diazenyl)-1H-tetrazole*, The 5th International Conference New Trends on

Sensing - Monitoring - Telediagnosis for Life Sciences NT-SMT-LS NOMARES Workshop, 3rd-4th July, 2020, Bucharest, Romania, Online, Poster (P.4.16.149).

4. Ioana-Georgiana Bugean, Elena Diacu, Eleonora-Mihaela Ungureanu, **Adinuța Păun**, Liviu Bîrzan, *Modified electrodes based on 4-(5-isopropyl-3,8-dimethylazulen-1-yl)-2,6-bis((E)-2-(thiophen-3-yl)vinyl)pyrylium perchlorate*, The 5th International Conference New Trends on Sensing - Monitoring - Telediagnosis for Life Sciences NT-SMT-LS NOMARES Workshop, 3rd-4th July, 2020, Bucharest, Romania, Online, Poster (P.4.4.137).
5. Ioana-Georgiana Bugean, **Adinuța Păun**, Elena Diacu, Eleonora-Mihaela Ungureanu, Liviu Bîrzan, *Modified electrodes based on 4-(azulen-1-yl)-2,6-bis((E)-2-(thiophen-2-yl)vinyl) pyrylium perchlorate for heavy metals detection*, CHIMIA 2020 - New Trends in Applied Chemistry, 27th-29th May, 2021, Constanța, Romania, Poster (PB19).
6. **Adina-Maria Păun**, Ovidiu-Teodor Matica, Alina-Giorgiana Brotea, Elena Diacu, Eleonora-Mihaela Ungureanu, *Spectroscopic and voltametric techniques for assessing the complexing capacity of E-5-((5-isopropyl-3,8-dimethylazulen-1-yl)dyazenyl)-1H-tetrazole of heavy metal cations*, CHIMIA 2020 - New Trends in Applied Chemistry, 27th-29th May, 2021, Constanța, Romania, Poster (PC4).
7. **Adina-Maria Păun**, Ovidiu-Teodor Matica, Laura-Bianca Enache, Elena Diacu, Eleonora-Mihaela Ungureanu, *Surface characterization of chemically modified electrodes based on E-5-((5-isopropyl-3,8-dimethylazulen-1-yl)dyazenyl)-1H-tetrazole for the evaluation of the complexation capacity of heavy metal ions*, RICCCE 22 - 22nd Romanian International Conference on Chemistry and Chemical Engineering 2022, WORKSHOP - New materials for electrochemical recognition of inorganic and biological species – NOMARES, 7th-9th September, 2022, Sinaia, Romania, Poster (S7-163).
8. Ovidiu-Teodor Matica, Elena Diacu, Alina-Giorgiana Brotea, **Adina-Maria Păun**, Amalia Ștefaniu, Eleonora-Mihaela Ungureanu, *DFT Investigations on 2-thioxo-thiazolidin-4-ones for Estimation of Chemical Reactivity Parameters*, RICCCE 22 - 22nd Romanian International Conference on Chemistry and Chemical Engineering 2022, WORKSHOP - New materials for electrochemical recognition of inorganic and biological species - NOMARES, 7th-9th September, 2022, Sinaia, Romania, Oral presentation.

# SELECTED BIBLIOGRAPHY

## Bibliography for Introduction

[1] *R. Singh, N. Gautam, A. Mishra and R. Gupta*, "Heavy metals and living systems: An overview", in Indian J. Pharmacol., **vol. 43,** no. 3, May-Jun. 2011, pp. 246-253.
[2] *M. F. Hughes*, "Arsenic toxicity and potential mechanisms of action", in Toxicol. Lett., **vol. 133**, no. 1, Jul. 2002, pp. 1-16.
[3] *R. A. Goyer, T. W. Clarkson*, Toxic Effects of Metals, Cassarett and Doull's Toxicology: The Basic Science of Poisons, McGraw-Hill, New York, 2001, pp. 811-867.
[4] *B. Welz, M. Sperling*, Atomic Absorption Spectrometry, 3rd ed., Wiley-VCH, Weinheim, 1999.
[5] *M. Montes-Bayon, K. DeNicola and J. A. Caruso, "*Liquid chromatography-inductively coupled plasma mass spectrometry", in J. Chromatogr. A, **vol. 1000**, no. 1-2, Jun. 2003, pp. 457-476.
[6] *E. H. Evans, J. A. Day, C. D. Palmer, W. J. Price, C. M. M. Smith and J. F. Tyson,* "Atomic spectrometry update. Advances in atomic emission, absorption and fluorescence spectrometry, and related techniques", in J. Anal. At. Spectrom., **vol. 20**, no. 6, May 2005, pp. 562-590.

[7] *Y. Zhang and S. B. Adeloju*, "Coupling of non-selective adsorption with selective elution for novel in-line separation and detection of cadmium by vapour generation atomic absorption spectrometry", in Talanta, **vol. 137**, May 2015, pp. 148-155.
[8] *A. K. Malik, V. Kaur and N. Verma*, "A review on solid phase microextraction-high performance liquid chromatography as a novel tool for the analysis of toxic metal ions", in Talanta, **vol. 68**, no. 3, Jan. 2006, pp. 842-849.
[9] *J. Wang, B. Tian, J. Wang, J. Lu, C. Olsen, C. Yarnitzky, K. Olsen, D. Hammerstrom and W. Bennett*, "Stripping analysis into the 21st century: faster, smaller, cheaper, simpler and better", in Anal. Chim. Acta, **vol. 385**, no. 1-3, Apr. 1999, pp. 429-435.
[10] *R. De Marco, G. Clarke and B. Pejcic*, "Ion-Selective Electrode Potentiometry in Environmental Analysis", in Electroanalysis, **vol. 19**, no. 19, Oct. 2007, pp. 1987-2001.
[11] *G.-O. Buică, I.-G. Lazăr, E. Saint-Aman, V. Tecuceanu, C. Dumitriu, A. A. Ivanov, A. B. Stoian and E.-M. Ungureanu*, "Ultrasensitive modified electrode based on poly(1H-pyrrole-1-hexanoic acid) for Pb(II) detection", in Sensors and Actuators B: Chemical, **vol. 246**, Jul. 2017, pp. 434-443.

## Bibliography for Chapter 4

[4.12] *E.-M. Ungureanu, A. C. Răzuș, L. Bîrzan, M.-Ș. Crețu and G.-O. Buică*, "Electrochemical study of azo-azulene compounds", in Electrochim. Acta, **vol. 53**, no. 24, Oct. 2008, pp. 7089-7099.
[4.15] *L. Bîrzan, M. Cristea, V. Tecuceanu, A. Hanganu, E.-M. Ungureanu and A. C. Răzuș*, "5-(Azulen-1-yldiazenyl)tetrazoles; Syntheses and Properties", in Rev. Chim., **vol. 71**, no. 5, 2020, pp. 251-264.
[4.16] *G.-O. Buică, I.-G. Lazăr, L. Bîrzan, C. Lete, M. Prodana, M. Enăchescu, V. Tecuceanu, A. B. Stoian and E.-M. Ungureanu*, "Azulene-ethylenediaminetetraacetic acid: A versatile molecule for colorimetric and electrochemical sensors for metal ions", in Electrochim. Acta, **vol. 263**, Febr. 2018, pp. 382-390.
[4.17] *L.-B. Enache, V. Anăstăsoaie, L. Bîrzan, E.-M. Ungureanu, P. Diao and M. Enăchescu*, "Polyazulene-Based Materials for Heavy Metal Ion Detection. 2. (E)-5-(azulen-1-yldiazenyl)-1H-Tetrazole-Modified Electrodes for Heavy Metal Sensing", in Coatings, **vol. 10**, no. 9, Sept. 2020, 869.
[4.19] *E. Cordoș, T. Frențiu, M. Ponta, A.-M. Rusu and E. Darvași*, Analiza prin spectrometrie de absorbție moleculară în ultraviolet-vizibil, Institutul Național de Optoelectronică, Bucharest, 2001, pp. 199-200.

## Bibliography for Chapter 5

[5.1] *E. Diacu, A. Păun, V. Anăstăsoaie, G.-L. Arnold-Tatu, L. Bîrzan and E.-M. Ungureanu*, "Electroactive properties of a new azulene thioxo-imidazolidin-4-one ligand for modified electrodes", in Journal of Electrochemical Science and Engineering, **vol. 10**, no. 2, Dec. 2019, pp. 209-217.
[5.2] *L.-B. Enache, V. Anăstăsoaie, L. Bîrzan, E.-M. Ungureanu, P. Diao and M. Enăchescu,* "Polyazulene-Based Materials for Heavy Metal Ion Detection. 2. (E)-5-(azulen-1-yldiazenyl)-1H-Tetrazole-Modified Electrodes for Heavy Metal Sensing", in Coatings, **vol. 10**, no. 9, Sept. 2020, 869.
[5.3] *M. D. Pop, O. Brîncoveanu, M. Cristea, G.-O. Buică, M. Enăchescu and E.-M. Ungureanu*, "AFM and SEM Characterization of Chemically Modified Electrodes Based on 5-[(azulen-1-yl)methylene]-2-thioxothiazolidin-4-one", in Rev. Chim., **vol. 68**, no. 12, 2018, pp. 2799-2803.
[5.4] *G.-O. Buică, I.-G. Lazăr, L. Bîrzan, C. Lete, M. Prodana, M. Enăchescu, V. Tecuceanu, A. B. Stoian and E.-M. Ungureanu*, "Azulene-ethylenediaminetetraacetic acid: A versatile molecule for colorimetric and electrochemical sensors for metal ions", in Electrochim. Acta, **vol. 263**, Febr. 2018, pp. 382-390.
[5.5] *R. A. Wilson and H. A. Bullen*, Introduction to Scanning Probe Microscopy (SPM), Basic Theory Atomic Force Microscopy (AFM), Department of Chemistry, Northern Kentucky University, Highland Heights, KY 41099.
[5.6] *V. Anăstăsoaie, C. Omocea, L.-B. Enache, L. Anicăi, E.-M. Ungureanu, J. F. van Staden and M. Enăchescu*, "Surface Characterization of New Azulene-Based CMEs for Sensing", in Symmetry, **vol. 13**, no. 12, Dec. 2021, 2292.

[5.7] *A.-M. Păun, O.-T. Matica, V. Anăstăsoaie, L.-B. Enache, E. Diacu and E.-M. Ungureanu*, "Recognition of Heavy Metal Ions by Using E-5-((5-Isopropyl-3,8-Dimethylazulen-1-yl)Dyazenyl)-1H-Tetrazole Modified Electrodes", in Symmetry, **vol. 13**, no. 4, Apr. 2021, 644.

## Bibliography for Chapter 6

[6.3] *A. C. Răzuș and L. Bîrzan*, "Synthesis of azulenic compounds substituted in the 1-position with heterocycles", in Monatsh Chem., **vol. 150**, Febr. 2019, pp. 139-161.
[6.16] *G.-O. Buică, E.-M. Ungureanu, L. Bîrzan, A. C. Răzuș and L.-R. Mandoc (Popescu)*, "Voltammetric sensing of lead and cadmium using poly(4-azulen-1-yl-2,6-bis(2-thienyl)pyridine) complexing films", in J. Electroanal. Chem., **vol. 693**, Mar. 2013, pp. 67-72.
[6.19] *A.-G. Brotea, O.-T. Matica, C. E. Musina (Borsaru) and E.-M. Ungureanu*, "Advanced materials based on 4-(azulen-1-yl)-2,6-bis((E)-2-(thiophen-2-yl)vinyl)pyridine", in U.P.B. Sci. Bull., series B, **vol. 84**, no. 3, 2022, pp. 53-62.
[6.25] *L. Bîrzan, M. Cristea, C. C. Drăghici, V. Tecuceanu, A. Hanganu, E.-M. Ungureanu and A. C. Răzuș*, "4-(Azulen-1-yl) six-membered heteroaromatics substituted in 2- and 6- positions with 2-(2-furyl)vinyl, 2-(2-thienyl)vinyl or 2-(3-thienyl)vinyl moieties", in Tetrahedron, **vol. 73**, no. 17, Apr. 2017, pp. 2488-2500.

## Bibliography for Chapter 7

[7.1] *J. W. Tukey*, Exploratory Data Analysis. In: The Concise Encyclopedia of Statistics, Springer, New York, NY, 2008.
[7.2] *S. H. C. du Toit, A. G. W. Steyn and R. H. Stumpf*, Graphical Exploratory Data Analysis, Springer-Verlag, New York, NY, 1986.
[7.5] *W. H. Kruskal and W. A. Wallis*, "Use of Ranks in One-Criterion Variance Analysis", in Journal of the American Statistical Association, **vol. 47**, no. 260, Dec. 1952, pp. 583-621.
[7.11] *C. D. Chiriță, C. Păunescu and D. Teaci*, Solurile României, Editura Agro-Silvică, Bucharest, 1967.